Part F
Supernova observations and analysis

Section 2: H-poor supernovae
(Type IIb/Ib/Ic/Ic-BL)

Stripped-envelope SNe : Fast rise (few weeks) and bright peak (~ 10^9 L_{sun})

Typically peak at a few times 10^{42} erg/s

Settle on radioactive tail after about 50d

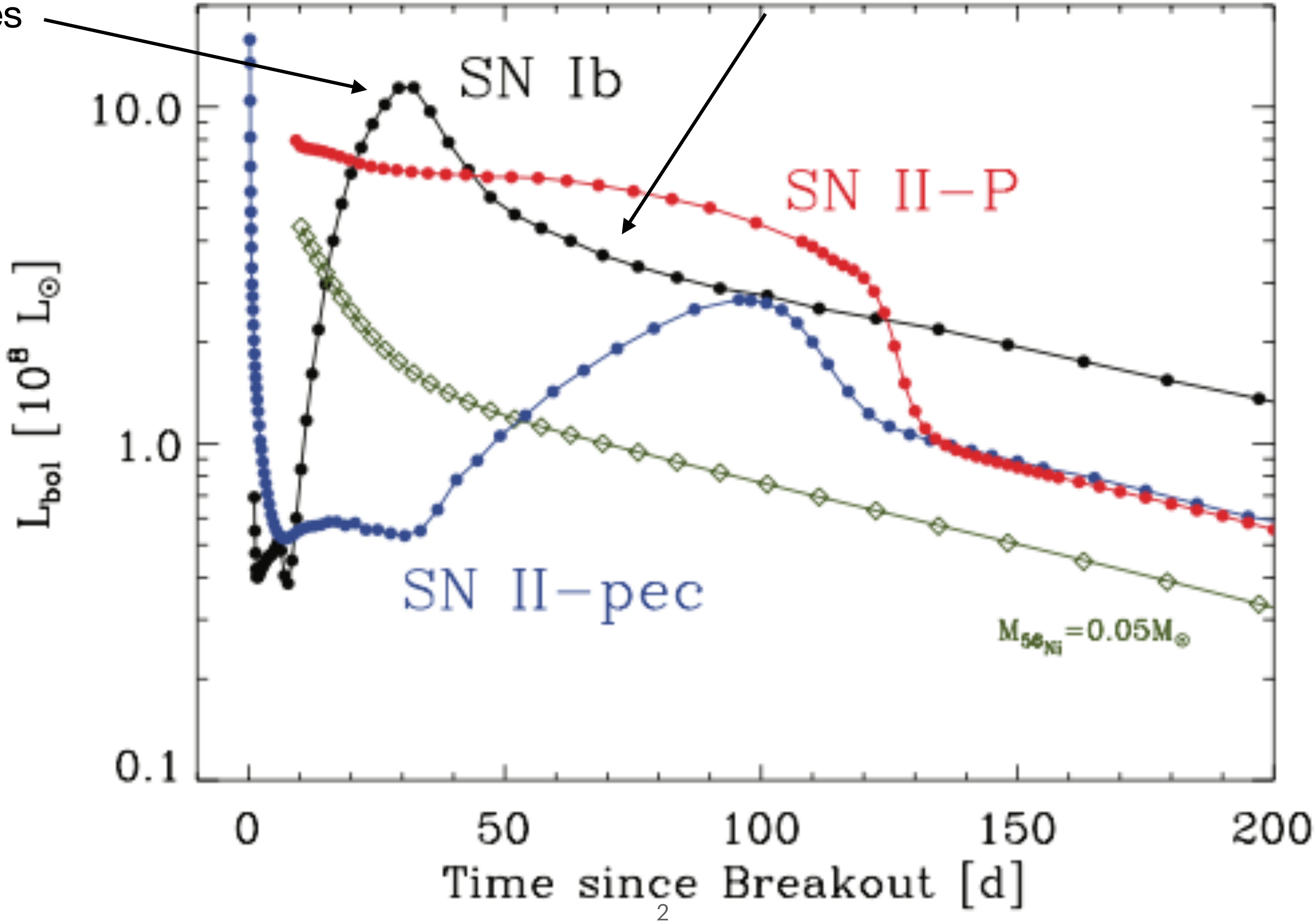

Dessart 2011

Characteristic dataset (SN 2009jf)

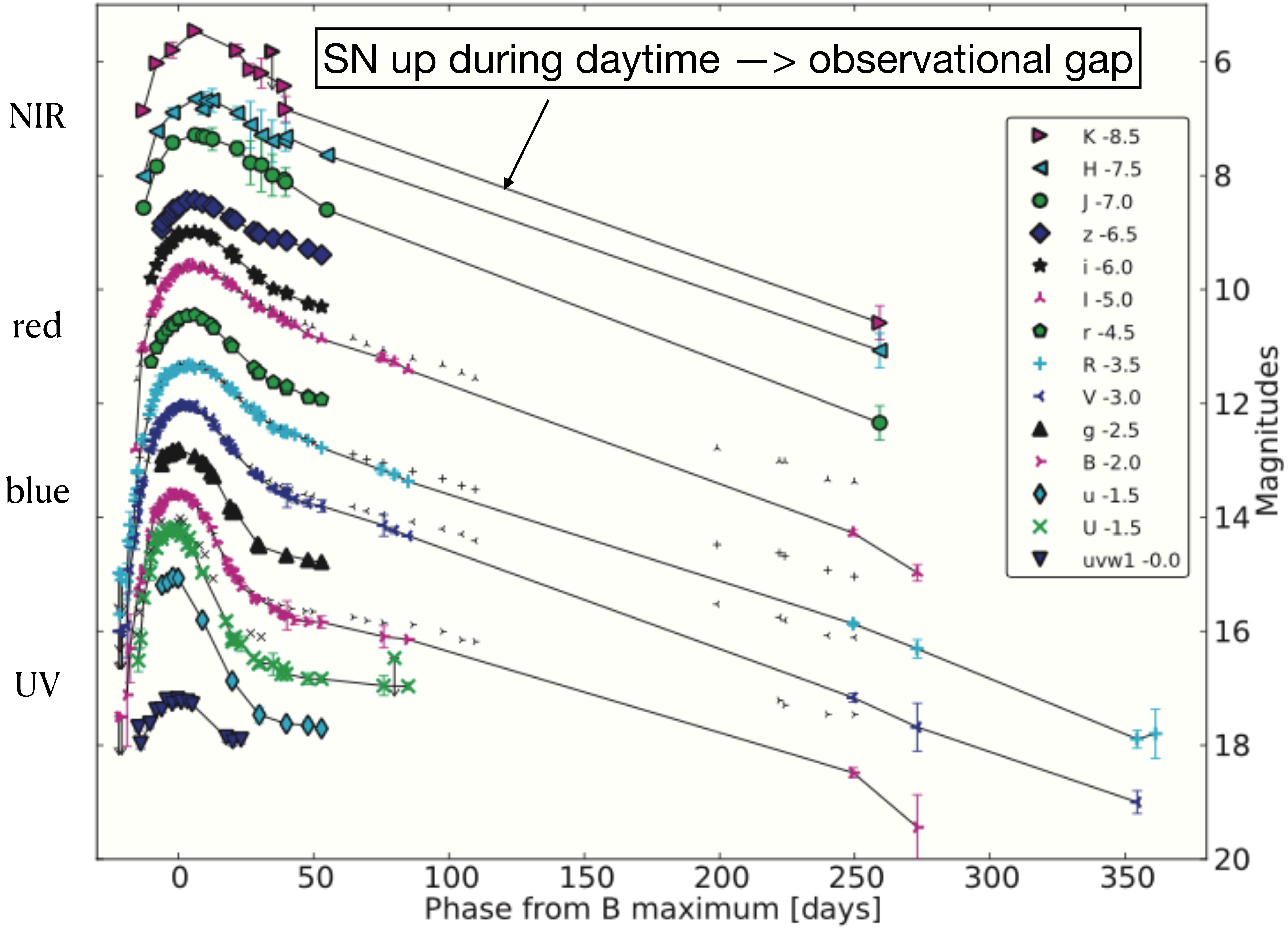

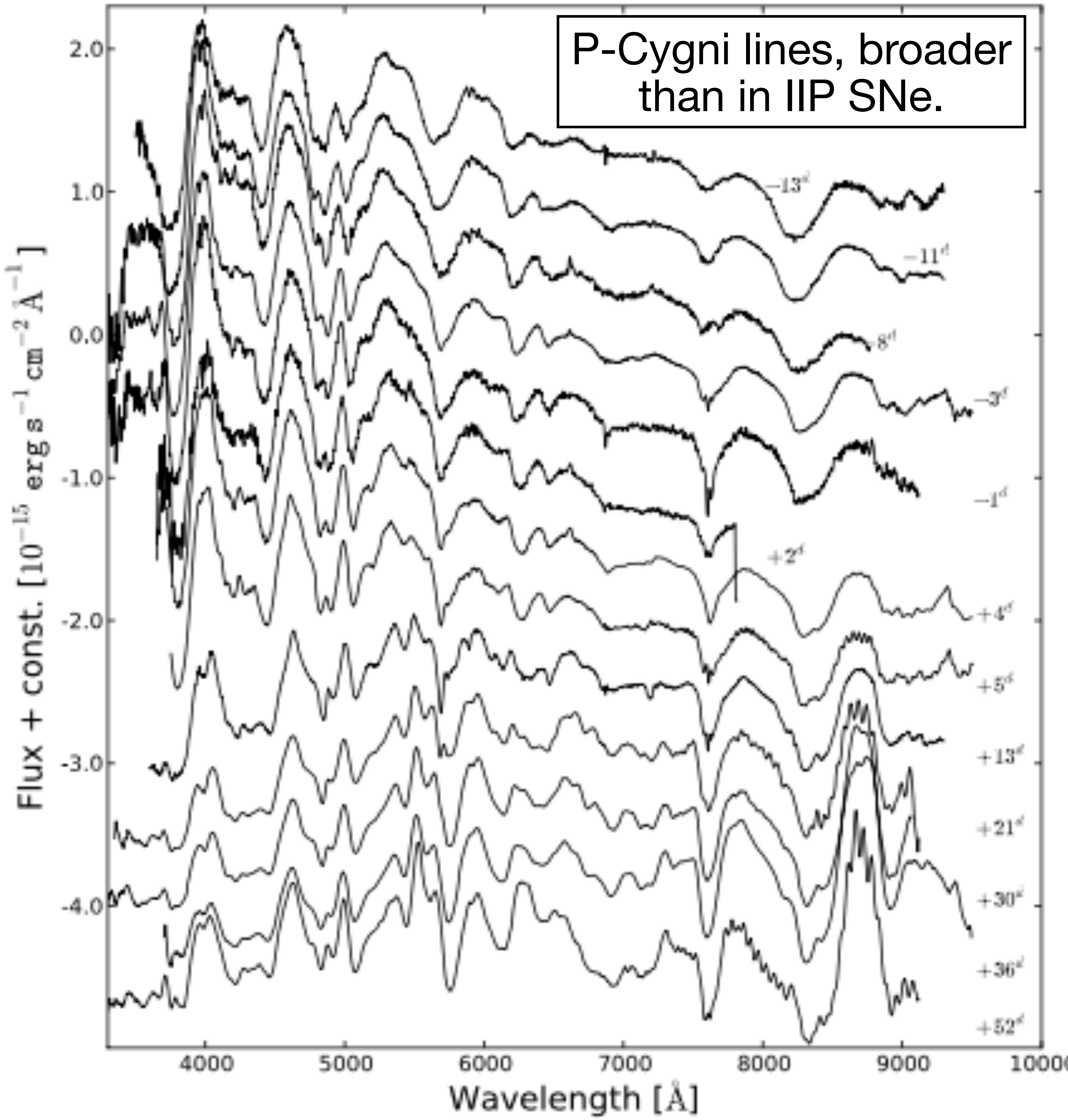

Valenti 2011

Stripped-envelope SN classes

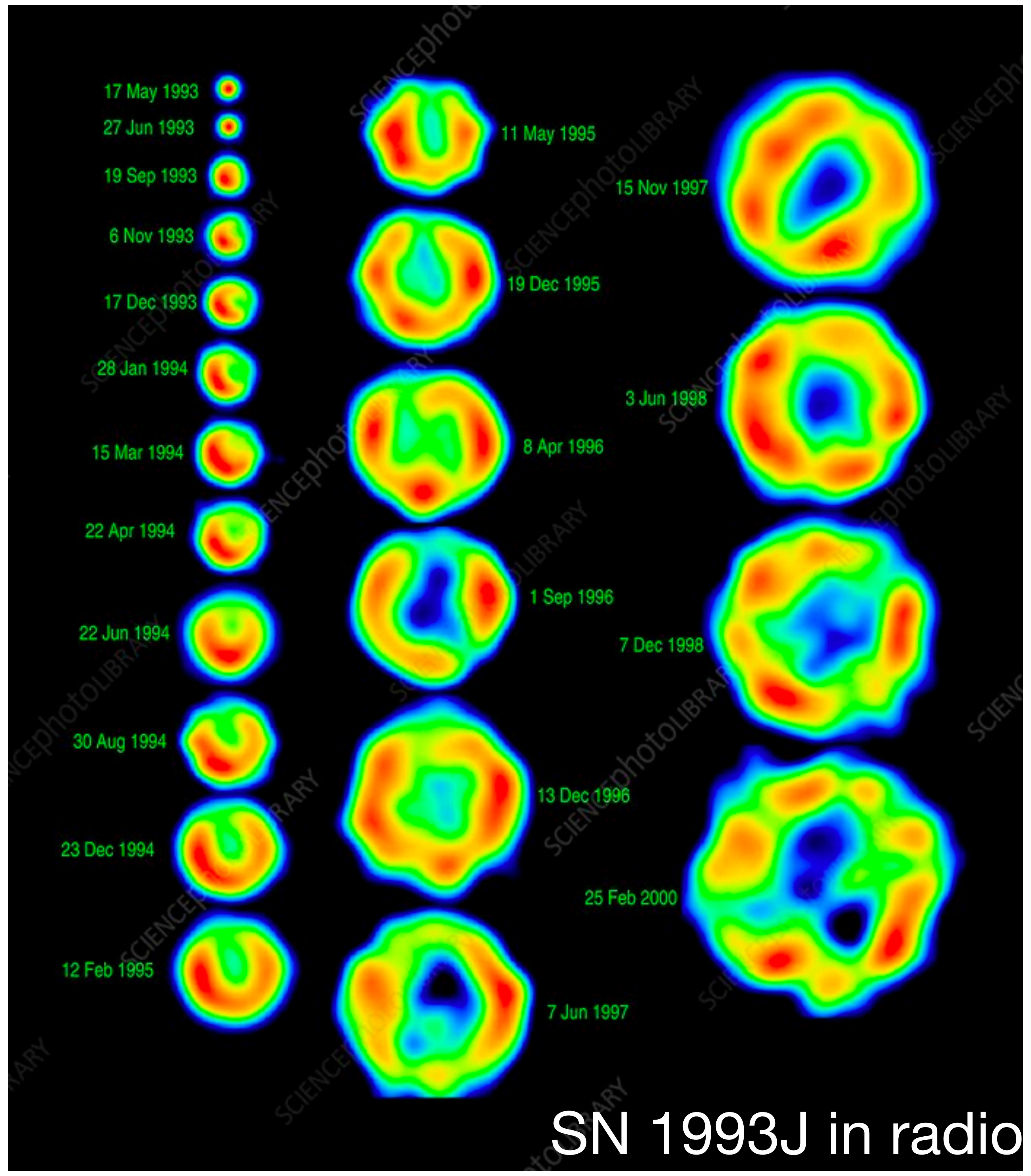

Type IIb

Weak H lines

Most famous:
SN 1993J

Type Ib

No H lines

Most famous:
SN 2008D

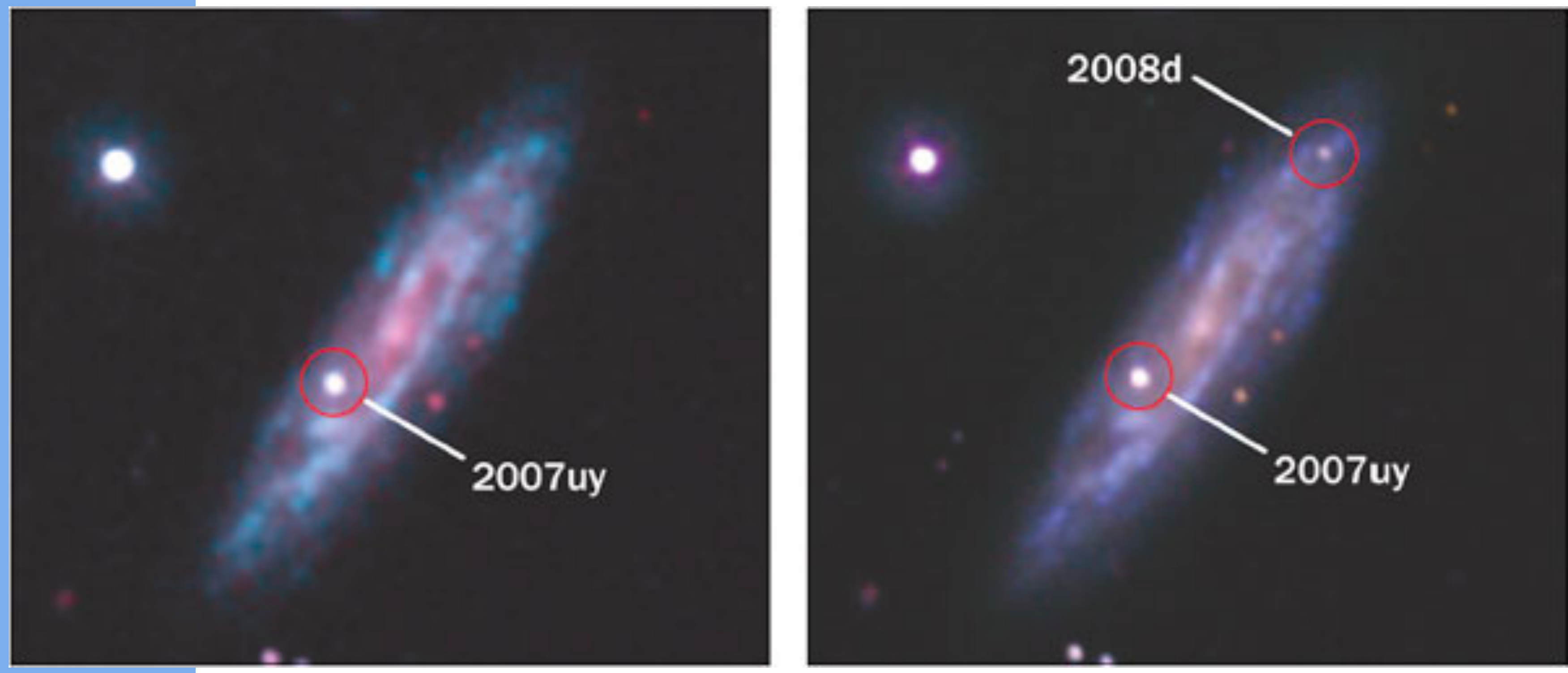

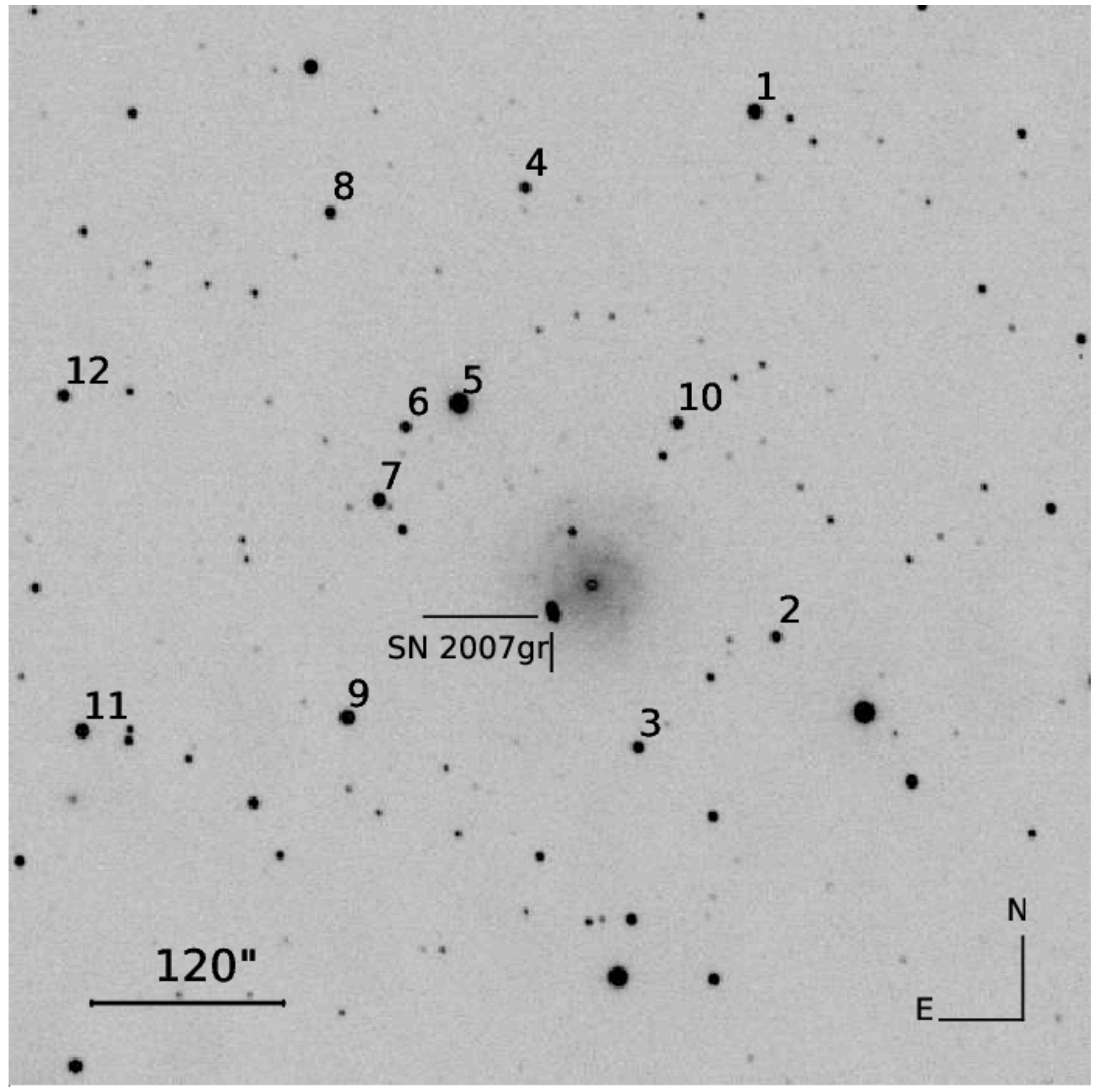

Type Ic

No H or He lines

Most famous:
SN 2007gr

Type Ic-BL

No H or He lines,
all lines broad

Most famous:
SN 1998bw

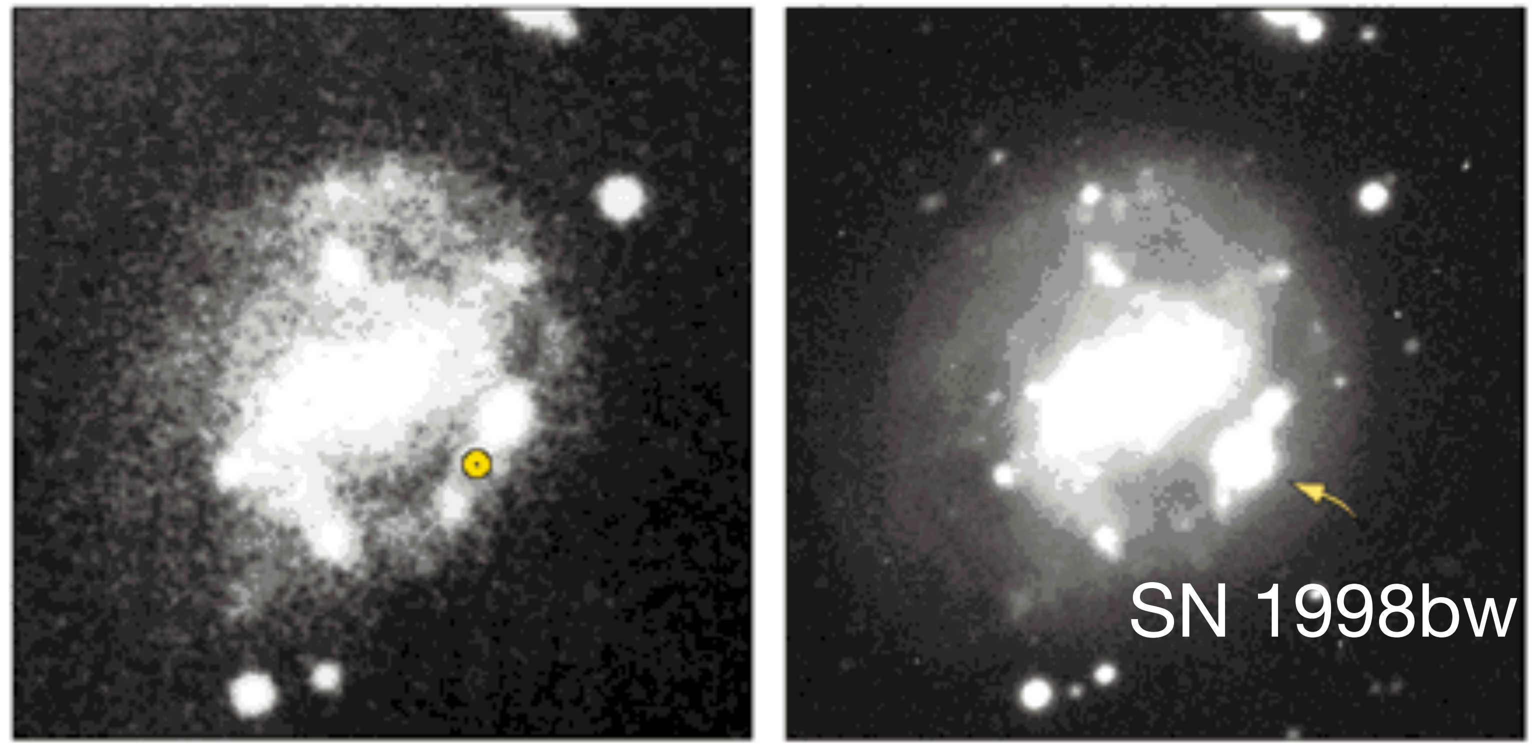

Spectral differences Type Ib vs Type Ic

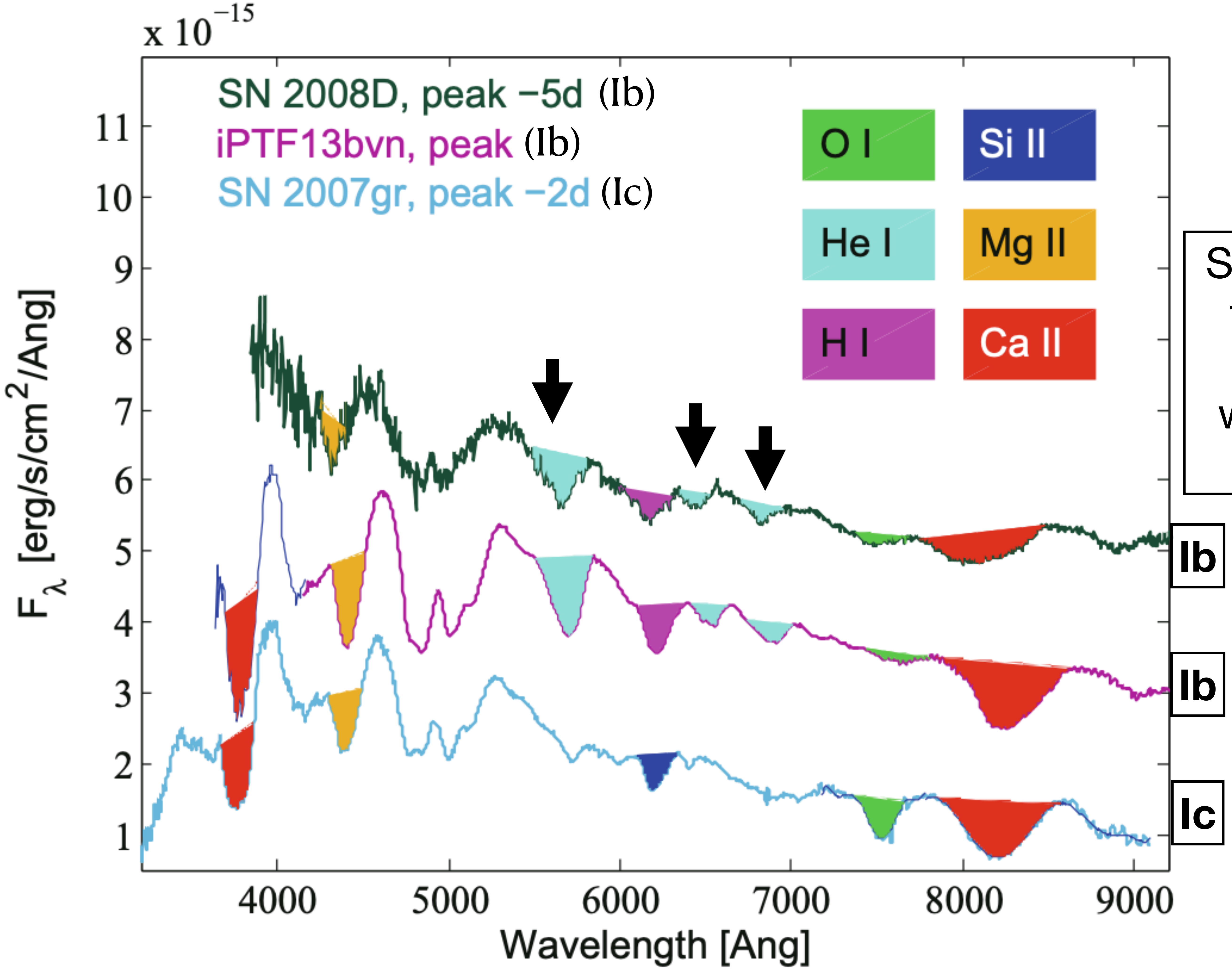

Search for P-Cygni absorption features (blue side of line) in three He lines with rest wavelengths 5876 Å, 6678 Å, and 7065 Å.

Gal-Yam 2017

Fig. 6 Spectra of events considered to be regular Type Ib SNe (*top*; SN 2008D from Modjaz et al. 2009 and iPTF13bvn from Cao et al. 2013) compared with a spectrum of a regular Type Ic SN (*bottom*; see Fig. 11). Major absorption features are marked, while the spectral shape in the *blue part* is dominated by multiple absorption features from iron-group elements

Spectral differences Ic vs Ic-BL

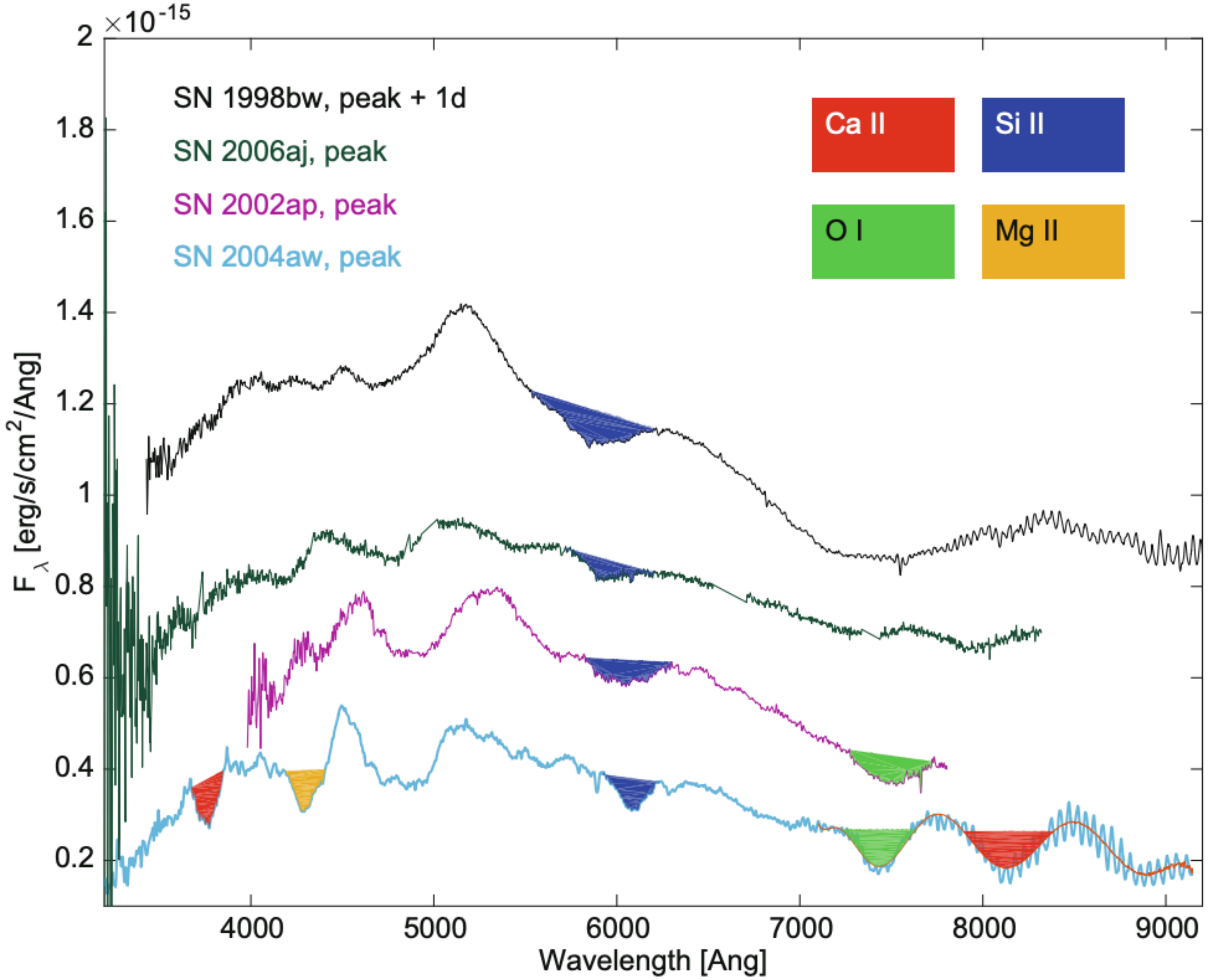

No firm definition of the "border" between Type Ic and Type Ic-BL : roughly when absorption at over 15,000 km/s is seen one uses Ic-BL.

Ic-BL

Ic

Fig. 12 A series of spectra of Type Ic SNe extending from SN 2004aw, considered a transitional event between normal and broad-line (BL) events (Taubenberger et al. 2006; Fig. 11), through the relatively low-energy SN 2002ap (Mazzali et al. 2002; spectrum from Gal-Yam et al. 2002), SN 2006aj, associated with an X-Ray Flash (XRF; Campana et al. 2006, spectrum from Pian et al. 2006) to the energetic SN 1998bw associated with GRB 980425 (Galama et al. 1998, spectrum from Patat et al. 2001). All spectra are around B-band peak. Note the gradual evolution from *bottom* to *top* as lines shift to higher velocities and blend together. This sequence establishes a spectral connection between the Ic-BL class and normal SNe Ic. A feature dominated by Si II is marked in all spectra, while other distinct features that are evident in normal SNe Ic (Fig. 11) blend together, for example the strong Ca II and OI features seen toward the *red*

Spectral differences IIb/Ib/Ic/Ic-BL

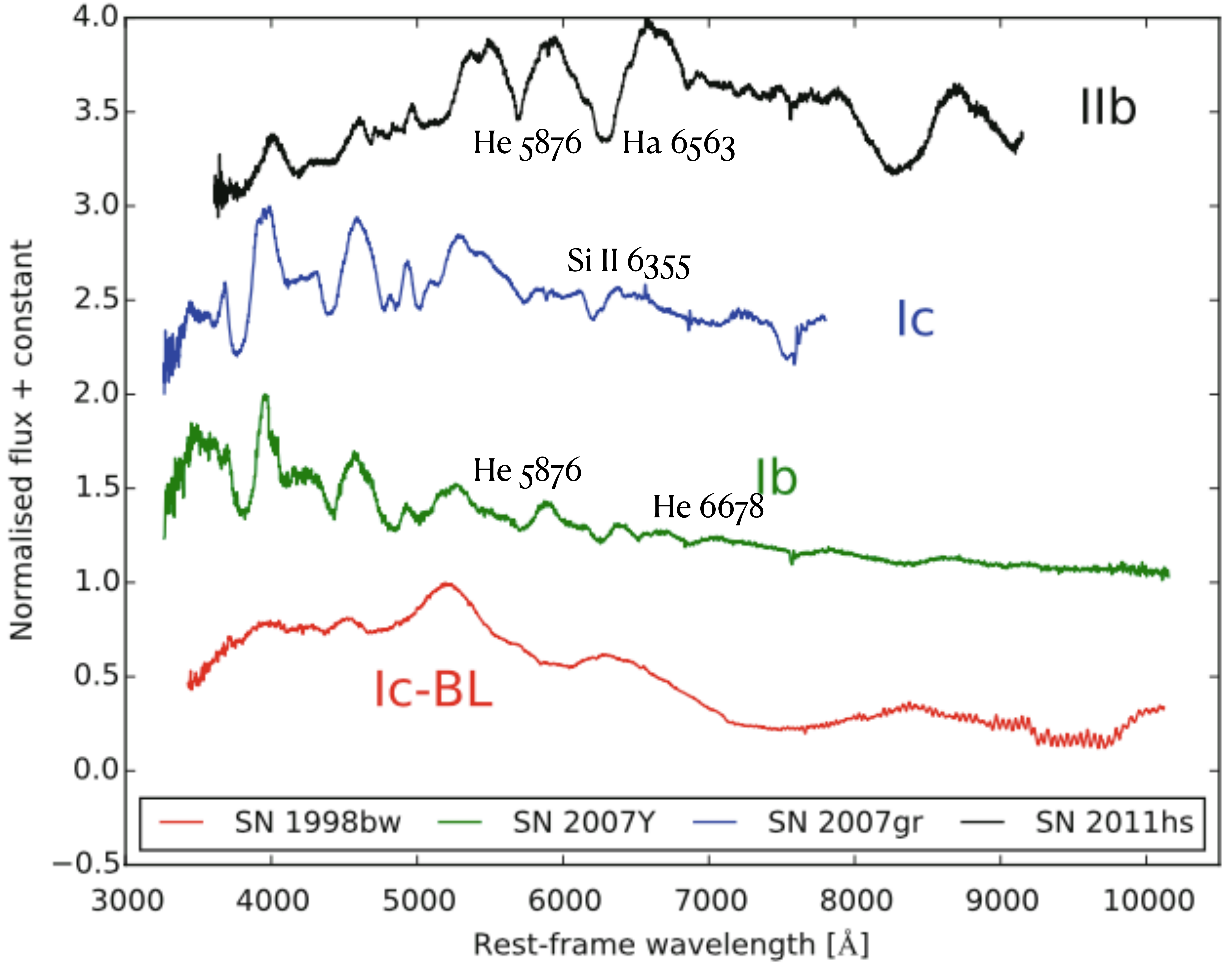

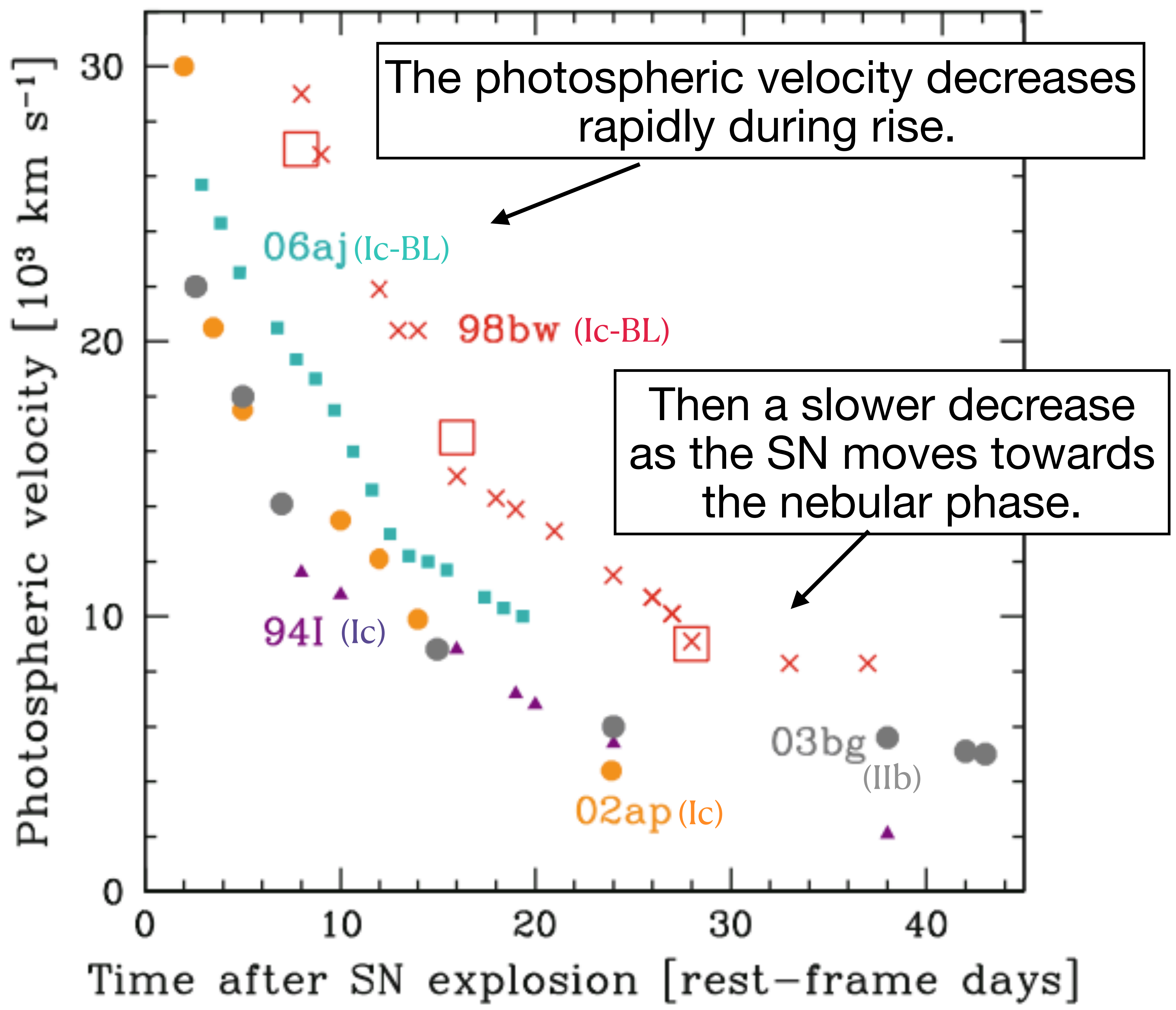

[Pian 2017](#)

Time evolution of P-Cygni minima

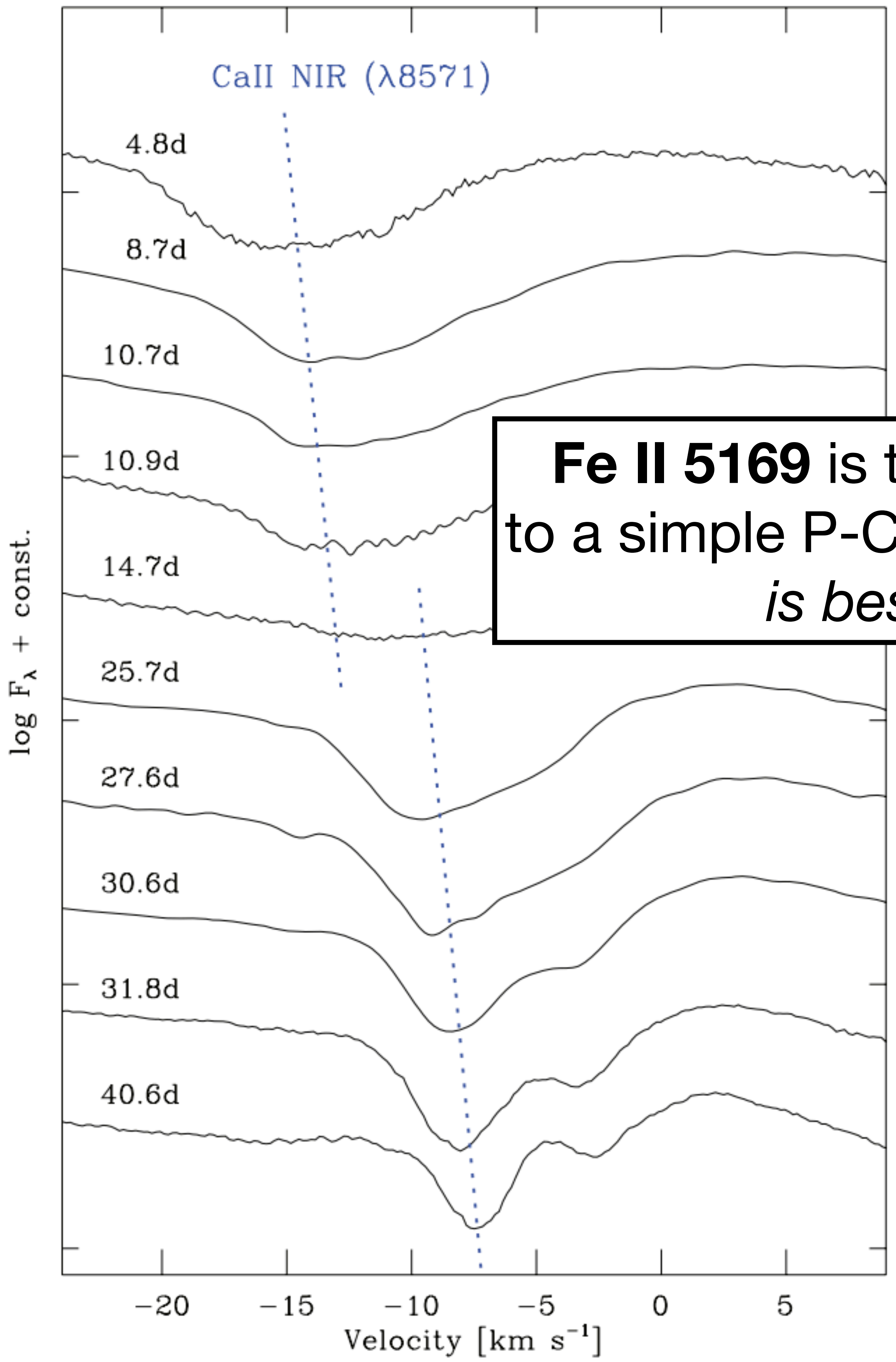

Figure 7. Evolution of the Ca II NIR line of SN 2008ax in velocity space. Velocities are measured with respect to 8571 Å. The flux is normalized to the local continuum and a constant shift is applied.

Fe II 5169 is the line operating closest to a simple P-Cygni model : *this minimum is best proxy for v_{phot}.*

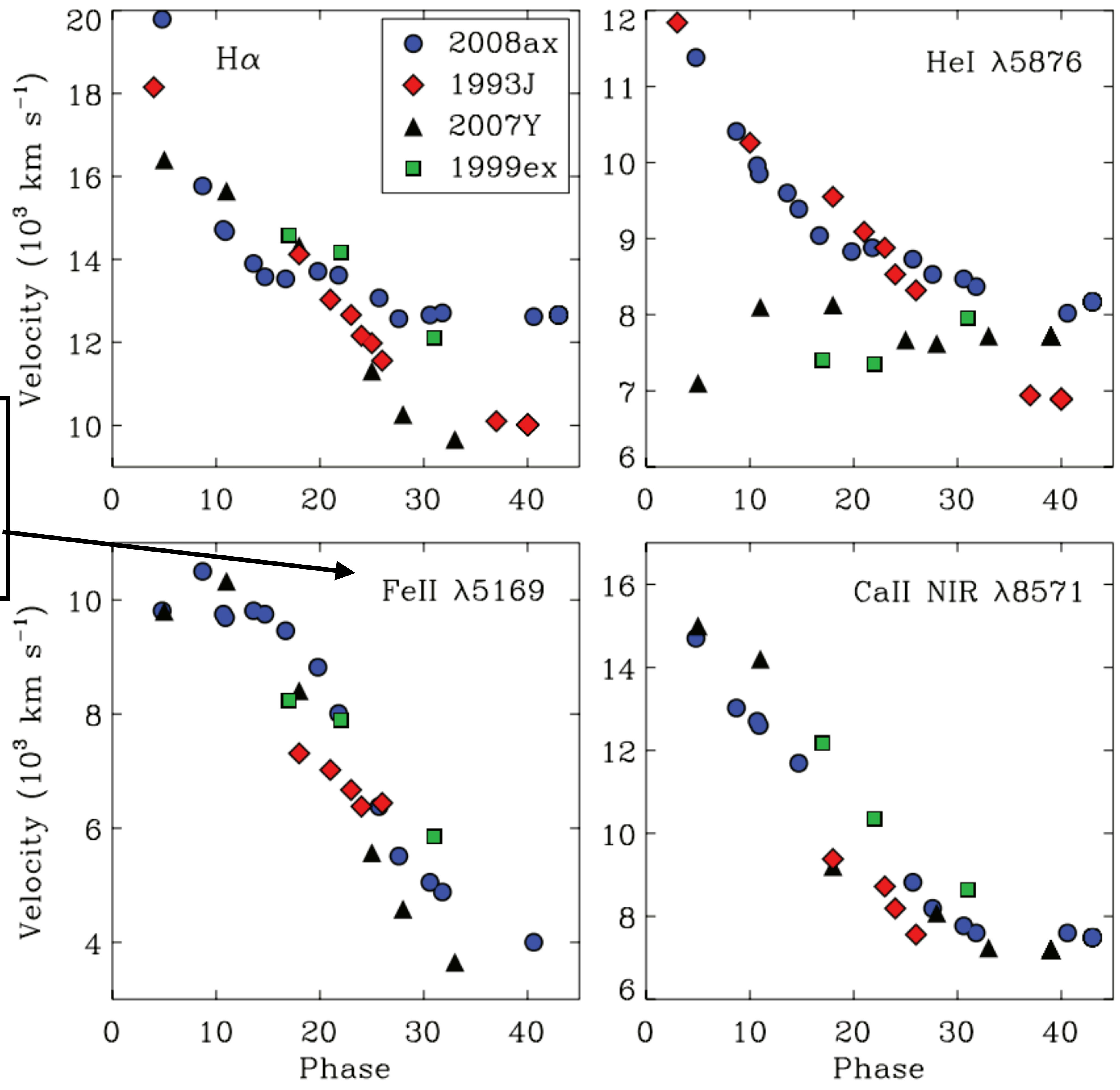

Figure 11. Evolution of Hα, He I λ5876, Fe II λ5169 and Ca II NIR line velocities. The data of SN 1993J are from Barbon et al. (1995) and Ohta et al. (1994), those of SN 1999ex are from Hamuy et al. (2002), and those of SN 2007Y are from Stritzinger et al. (2009). The Hα identification in SN 1999ex is only tentative. The phase is computed with respect to the explosion time.

Taubenberger 2011

Stripped-envelope SN light curves

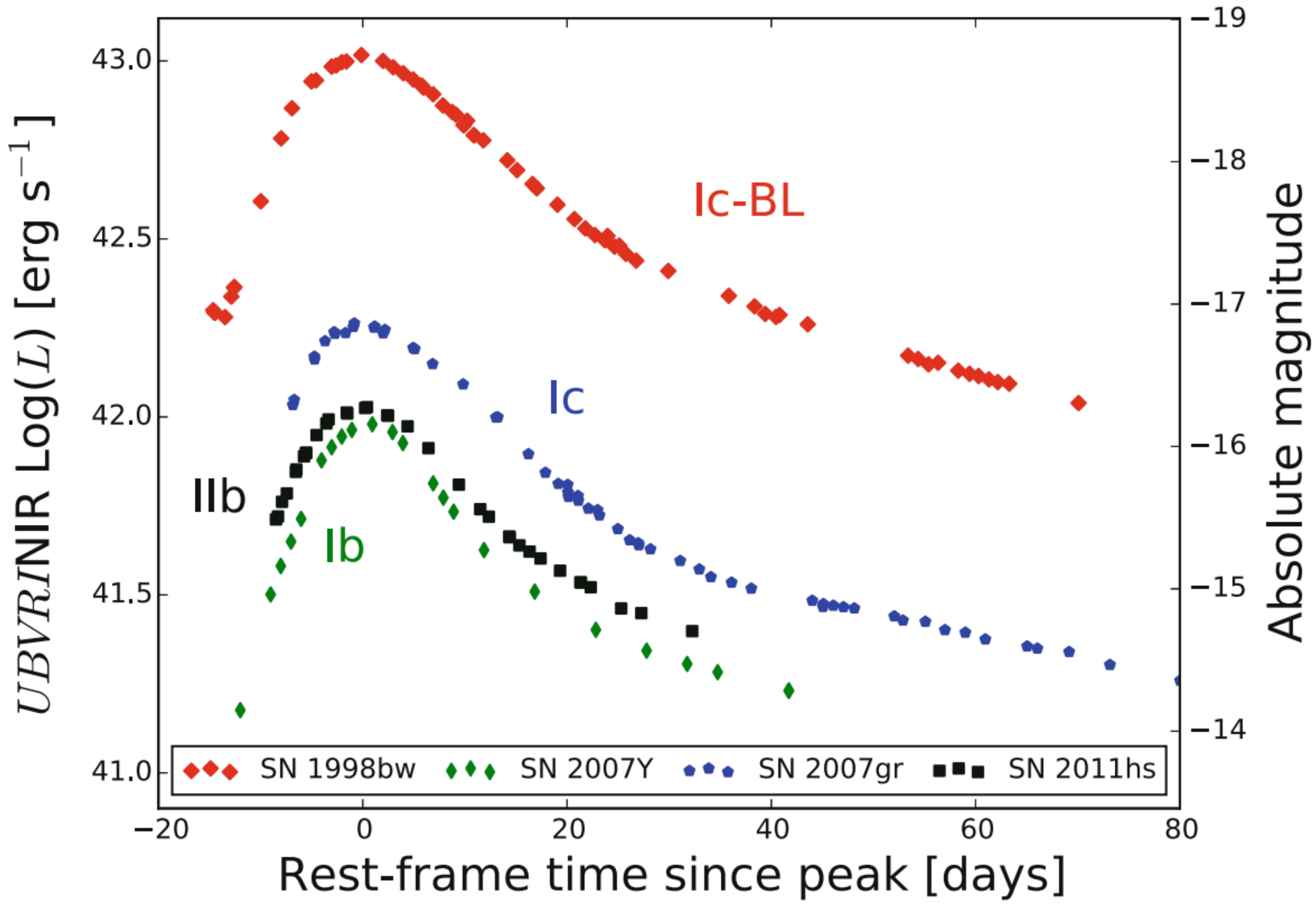

Fig. 1 Pseudo-bolometric light curves of representative stripped-envelope core-collapse SNe of different types based on observations with optical and near-infrared filters

Rise time is a few weeks.

Peak luminosity : log L = 42 - 43 erg/s.

Discussion points:

1) What does it tell us that Ic-BL SNe are both brighter and have higher velocities?

2) What could differ between Ib and Ic progenitors?

Pian 2017

Stripped-envelope SN light curves

Sometimes a **"cooling phase"**
(powered by shock deposited energy) seen. Can diagnose R_0.

But for most SNe the light curve is already rising
(^{56}Ni-powered diffusion phase has begun) within a few days
of the explosion.

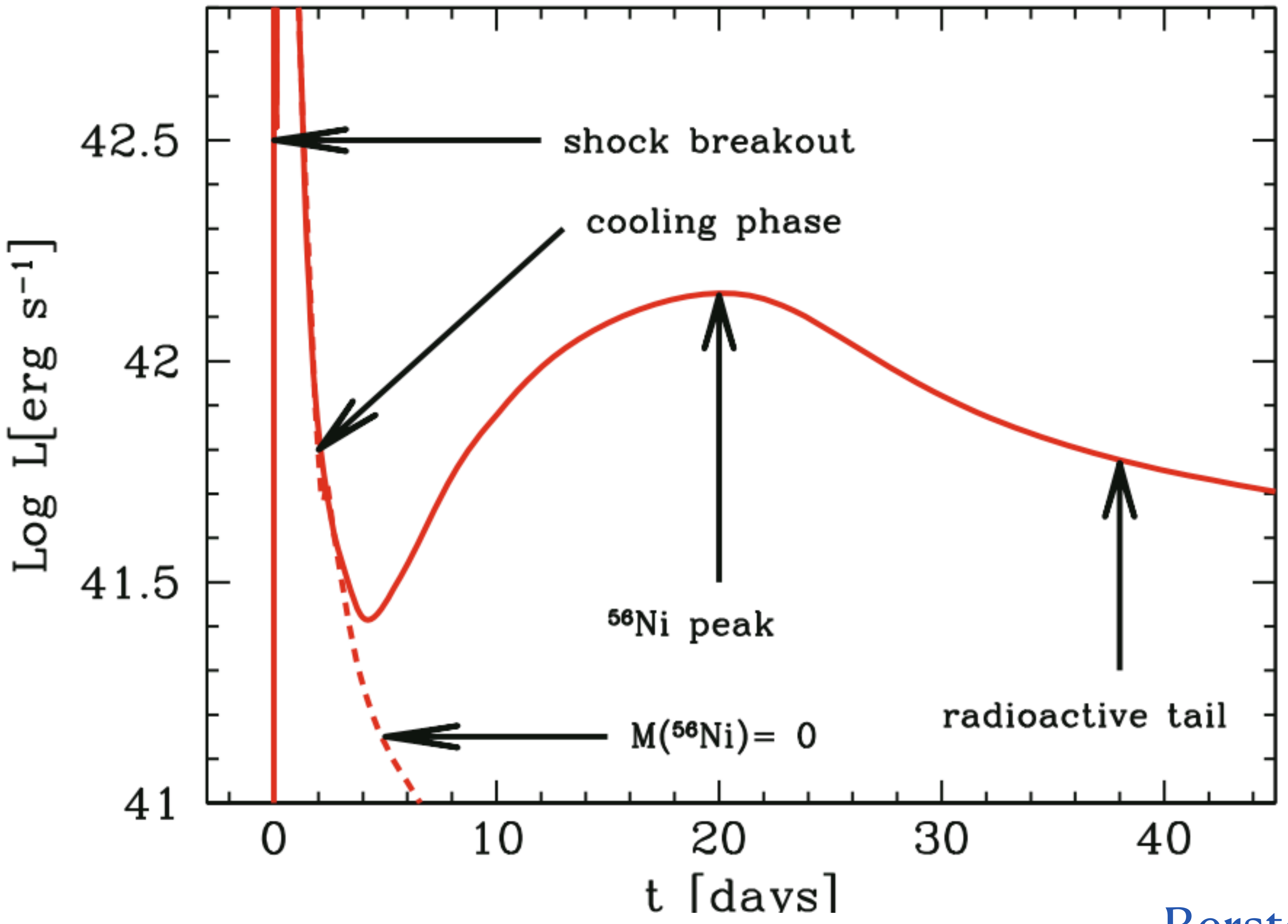

Bersten 2017

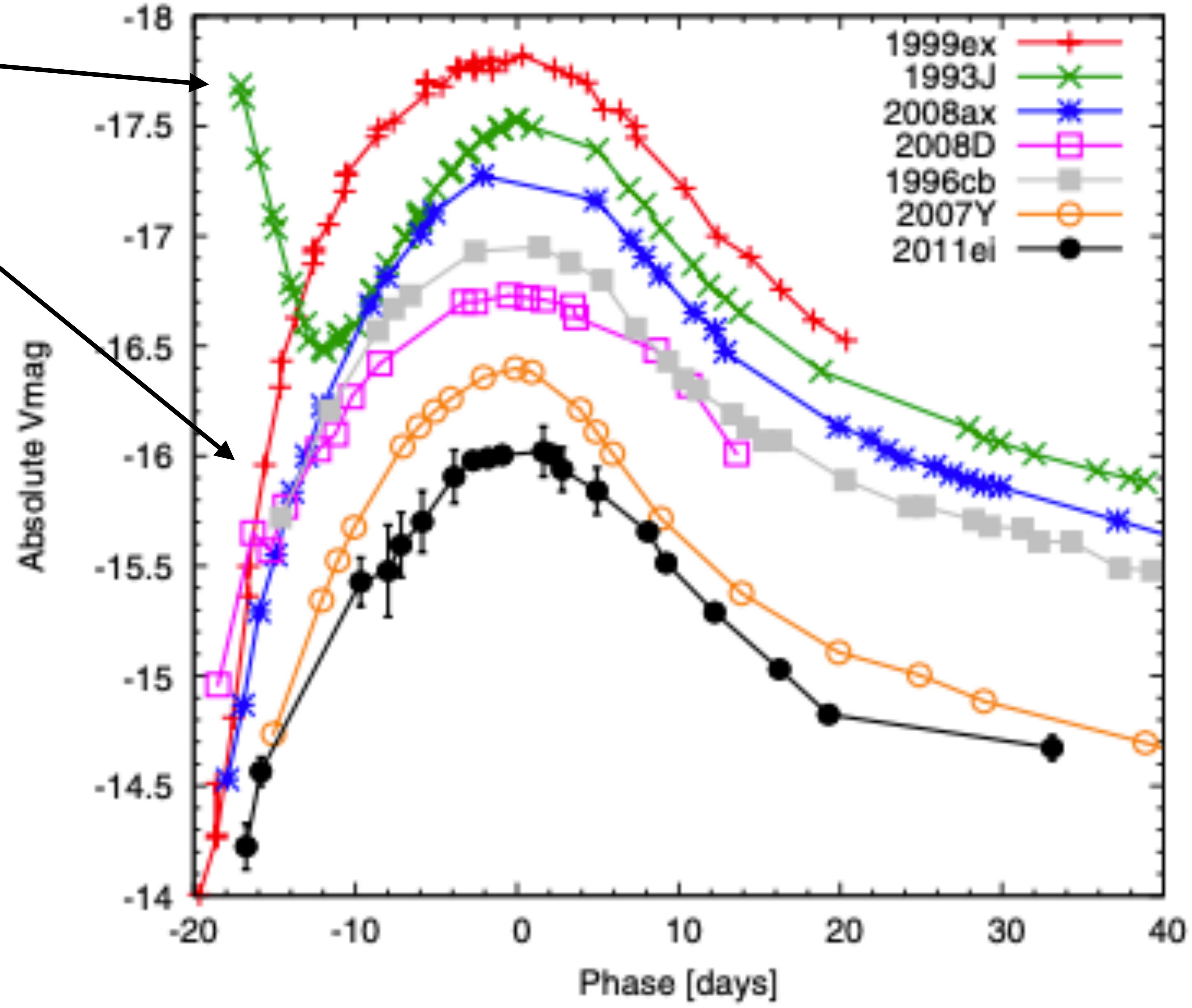

Milisavjlevic 2013

IIb/Ib/Ic SNe have **similar peak brightness distributions**.
Ic-BL tend to be brighter.

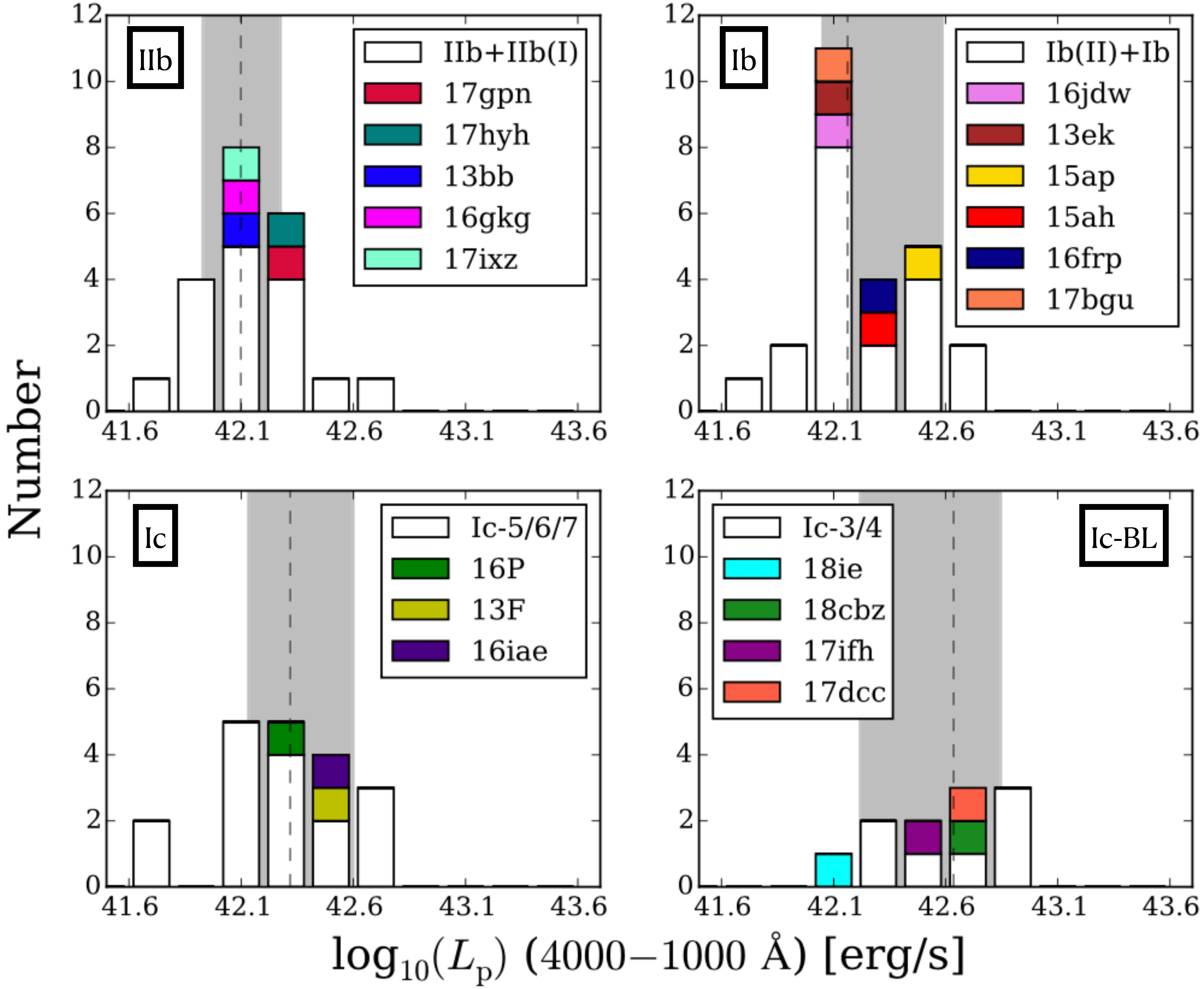

Prentice 2019

No differences in **light curve width** distributions between IIb/Ib/Ic/Ic-BL SNe

$t_{-1/2} \sim 10d$

$t_{+1/2} \sim 15d$

→ $FWHM \sim \Delta t \sim 25d$

Factor ~2 variation in light curve width.

A higher $t_{-1/2}$ correlates with a higher $t_{+1/2}$ (not shown here).

Table 6. Median temporal values derived from the *BVRI* data.

Type	$t_{-1/2}$ (d)	$t_{+1/2}$ (d)	Width (d)
SNe Ic-BL/GRB-SNe	$8.6\pm^{1.9}_{1.1}$	$15.1\pm^{1.0}_{2.0}$	$24.7\pm^{2.7}_{2.3}$
SNe Ic	$9.3\pm^{2.6}_{1.1}$	$19.2\pm^{4.7}_{5.4}$	$23.8\pm^{7.3}_{5.4}$
SNe Ib	$11.2\pm^{2.2}_{1.4}$	$17.0\pm^{2.8}_{2.9}$	$26.4\pm^{3.6}_{3.9}$
SNe IIb	$10.1\pm^{1.2}_{0.4}$	$15.3\pm^{2.8}_{1.6}$	$25.4\pm^{2.3}_{0.8}$

Prentice 2016, 2019

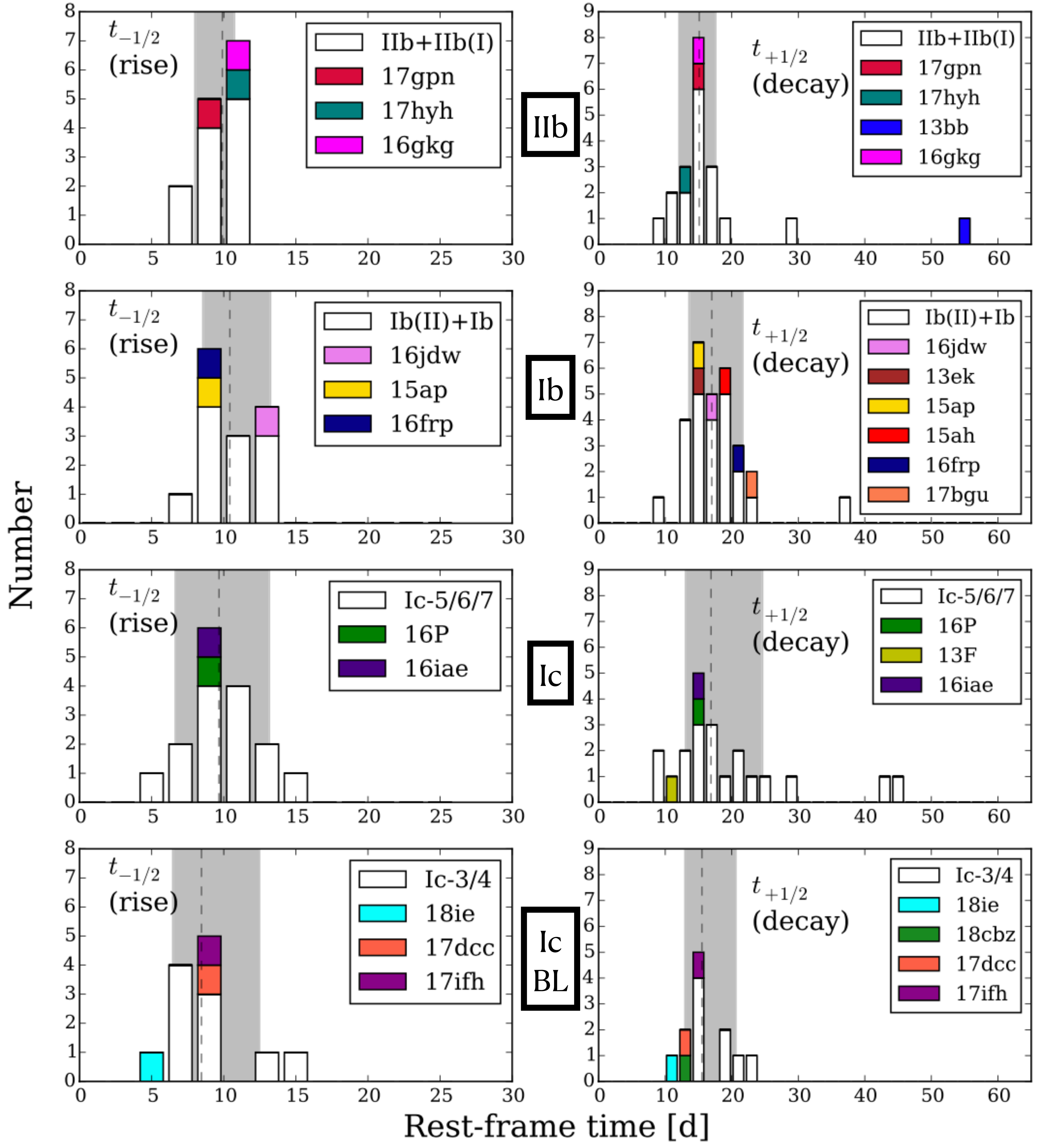

No differences between classes in late-time declines rates

Exercise set 2 : calculate the minimum and maximum possible decline rates.

What does a typical decline rate of 0.017 mag/day tell us?

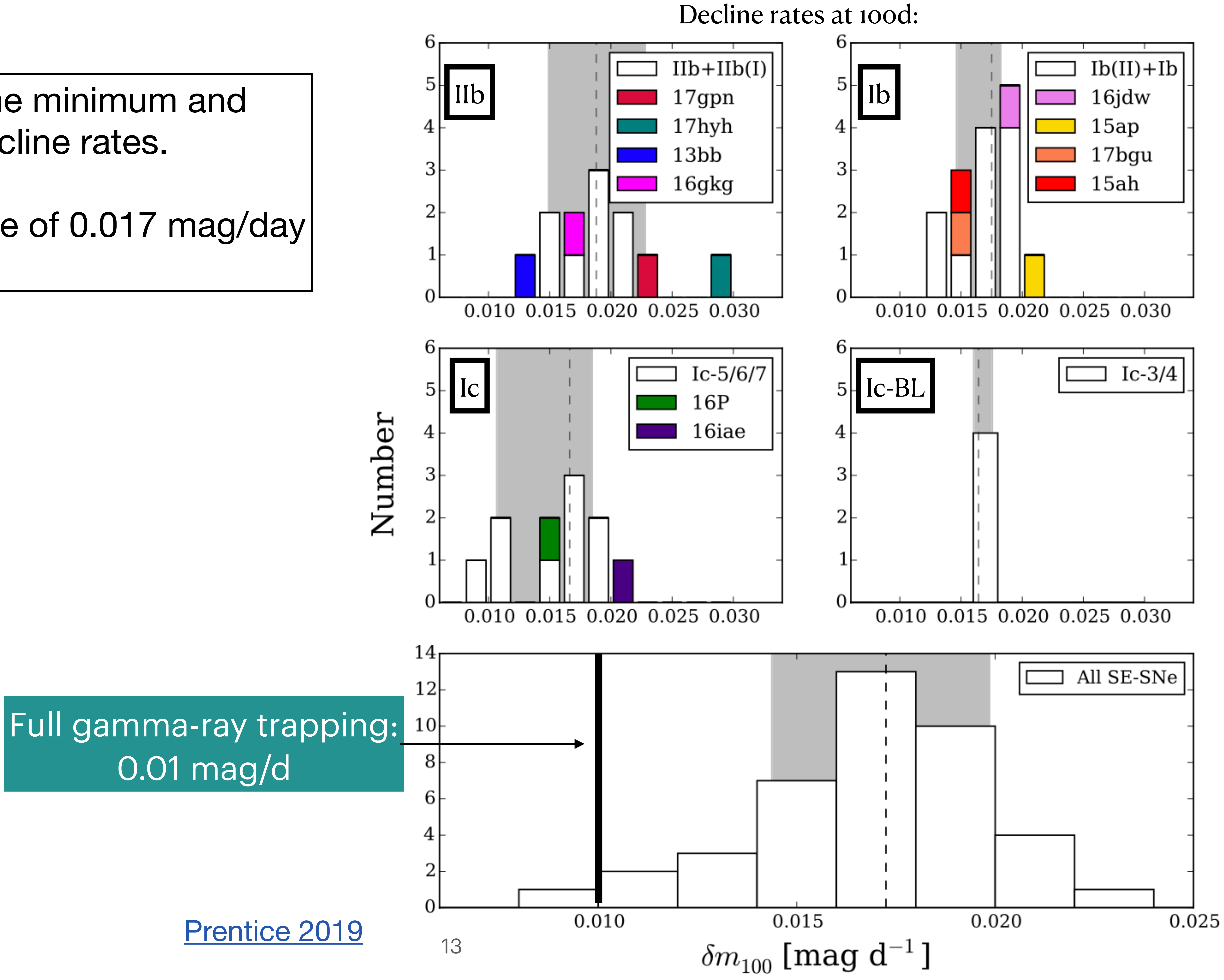

[Prentice 2019](#)

From diffusion phase light curves: ejecta masses of $1 - 5\ M_\odot$ inferred

Our light curve duration formula from Part E:

$\Delta t \approx 20\text{d}\ E_{51}^{-1/4} M_{M\odot}^{3/4} \kappa_{0.2}^{1/2}$

From spectra, singly or doubly ionized species —> $\kappa \approx 0.05$ cm^2 g^{-1}

$\Delta t = 25d, \kappa = 0.05$ cm^2 g^{-1} $\rightarrow M = 3.5\ M_\odot \times E_{51}^{1/3}$

One may try to eliminate E_{51} by linking M and E by measured $v_{phot}(t)$, but quite difficult to get a robust result.

No clear difference in ejecta mass inferred between the classes.

Advanced model fittings give similar results.

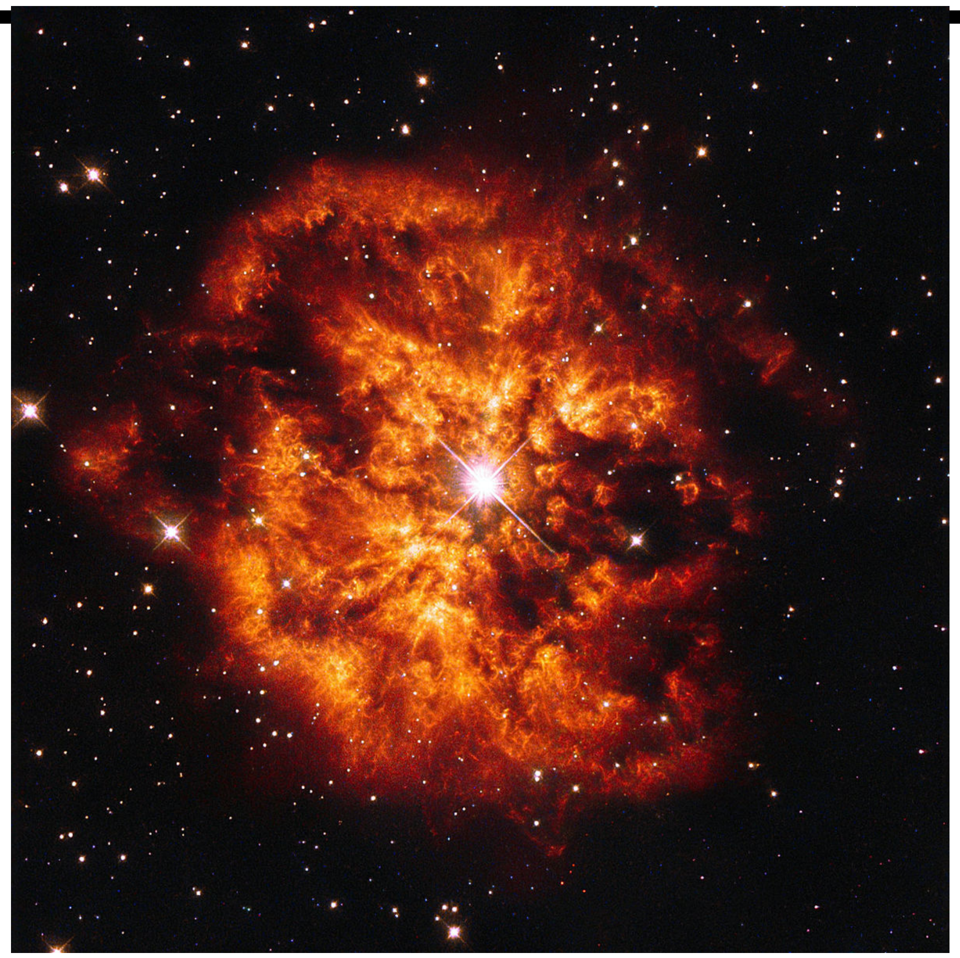

Inferred Type Ibc ejecta masses are 1-5 M_{sun}: Not explosion of massive Wolf-Rayet stars?

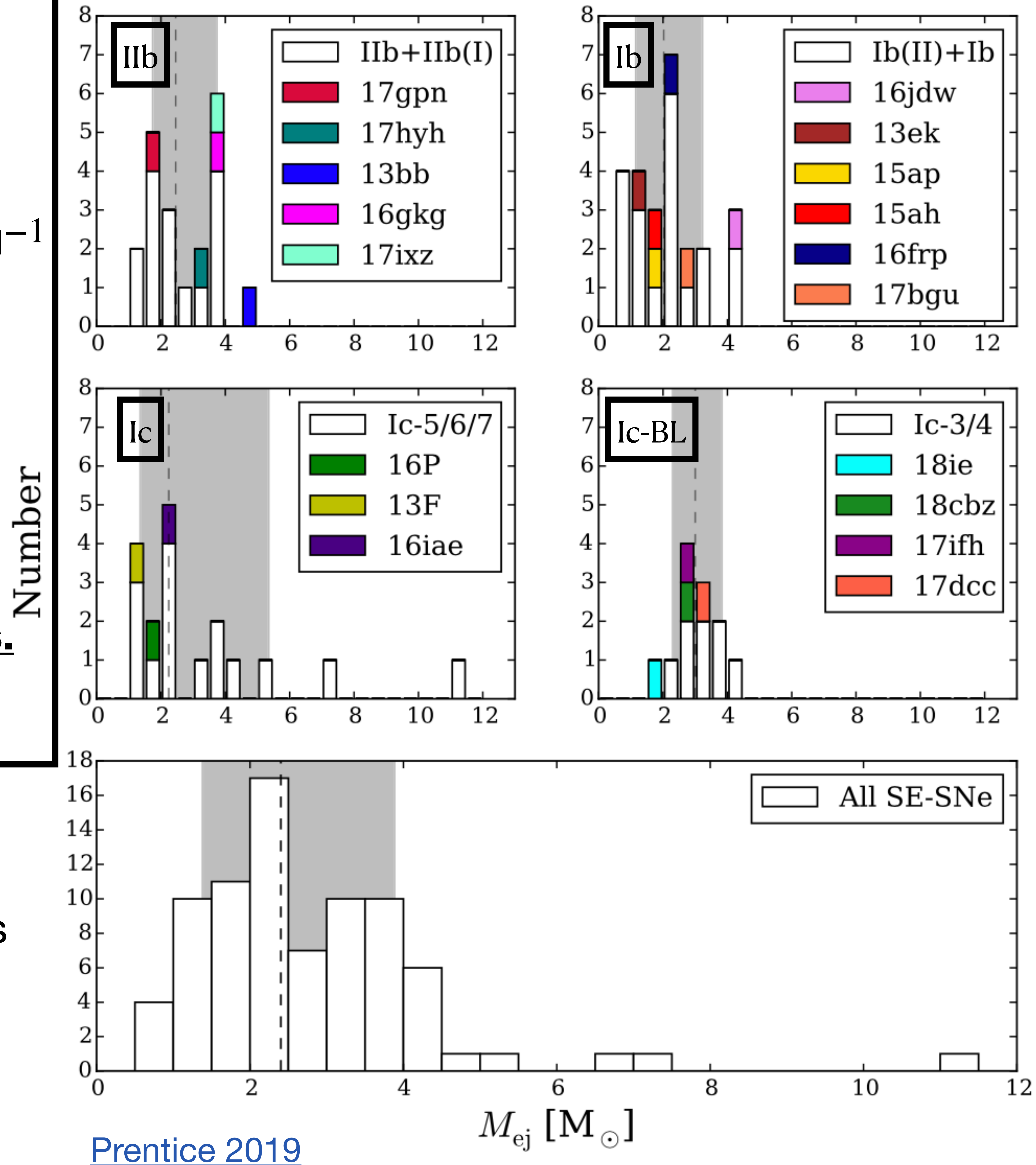

Prentice 2019

Ejecta masses of $1 - 5\ M_\odot$ inferred

Table 7
Sample Averages

SN Type	$M_{V_{peak}}$ (mag)	$M_{R_{peak}}$ (mag)	M_{Ni} ($M_\odot$)	τ_c (days)	$M_{ej}^{3/4} E_K^{-1/4}$ $((10^{51} erg)^{-1/4} (M_\odot)^{3/4})$	M_{ej}[a] ($M_\odot$)	E_K[a] (10^{51} erg)
SNe Ib	-17.6 ± 0.9	-17.9 ± 0.9	0.20 ± 0.16	13 ± 3	1.7 ± 0.3	$2.0^{+1.1}_{-0.8}$	$1.2^{+0.7}_{-0.5}$
SNe Ic	-18.0 ± 0.5	-18.3 ± 0.6	0.24 ± 0.15	12 ± 4	1.5 ± 0.4	$1.7^{+1.4}_{-0.9}$	$1.0^{+0.9}_{-0.5}$
SNe Ic-BL	-18.3 ± 0.8	-19.0 ± 1.1	0.58 ± 0.55	14 ± 3	1.7 ± 0.4	$4.7^{+2.3}_{-1.8}$	11^{+6}_{-4}
Engine-driven SNe	-18.9 ± 0.3	-18.9 ± 0.4	0.40 ± 0.18	12 ± 3	1.5 ± 0.3	$3.6^{+2.0}_{-1.6}$	$9.0^{+5.0}_{-4.0}$

Note. [a] Typical photospheric velocities of $v_{ph} = 10{,}000\ \mathrm{km\,s^{-1}}$ are assumed for SNe Ib and Ic and $v_{ph} = 20{,}000\ \mathrm{km\,s^{-1}}$ for SNe Ic-BL and engine-driven SNe.

Drout 2011

Individual studies sometimes finds differences between the classes, but no such difference has been consistently confirmed by multiple studies.

Table 6. Average v_{ph} and explosion parameters for SE SN types.

SN type	v_{ph} (km s^{-1}) Mean	v_{ph} Sth. dev.	M_{Ni} ($M_\odot$) Mean	M_{Ni} Std. dev.	M_{ej} ($M_\odot$) Mean	M_{ej} Sth. dev.	E_K (10^{51} erg) Mean	E_K Sth. dev.
IIb	8300	750	0.11	0.04	2.2	0.8	1.0	0.6
Ib	9900	1400	0.17	0.16	2.6	1.1	1.6	0.9
Ic	10 400	1200	0.22	0.16	3.0	2.8	1.9	1.3
Ic-BL	19 100	5000	0.32	0.15	2.9	2.2	6.0	5.0

Lyman 2016

SESNe appear to produce more ^{56}Ni than Type II SNe.
Ic-BL SNe may make more ^{56}Ni than the other subclasses.

Table 10. Median values for the fully bolometric sample.

SN Type	$\log(Lp)$	M_{Ni} ($M_\odot$)
Ic-BL/GRB-SNe	$43.00\pm^{0.21}_{0.21}$	$0.34\pm^{0.13}_{0.19}$
Ic	$42.51\pm^{0.06}_{0.36}$	$0.16\pm^{0.03}_{0.10}$
Ib	$42.50\pm^{0.10}_{0.20}$	$0.14\pm^{0.04}_{0.04}$
IIb	$42.36\pm^{0.26}_{0.11}$	$0.11\pm^{0.04}_{0.04}$

Prentice 2016

Modelling SESN light curves

As for SN 1987A, in many cases is **significant mixing** of ^{56}Ni needed to make good-fitting light curves.

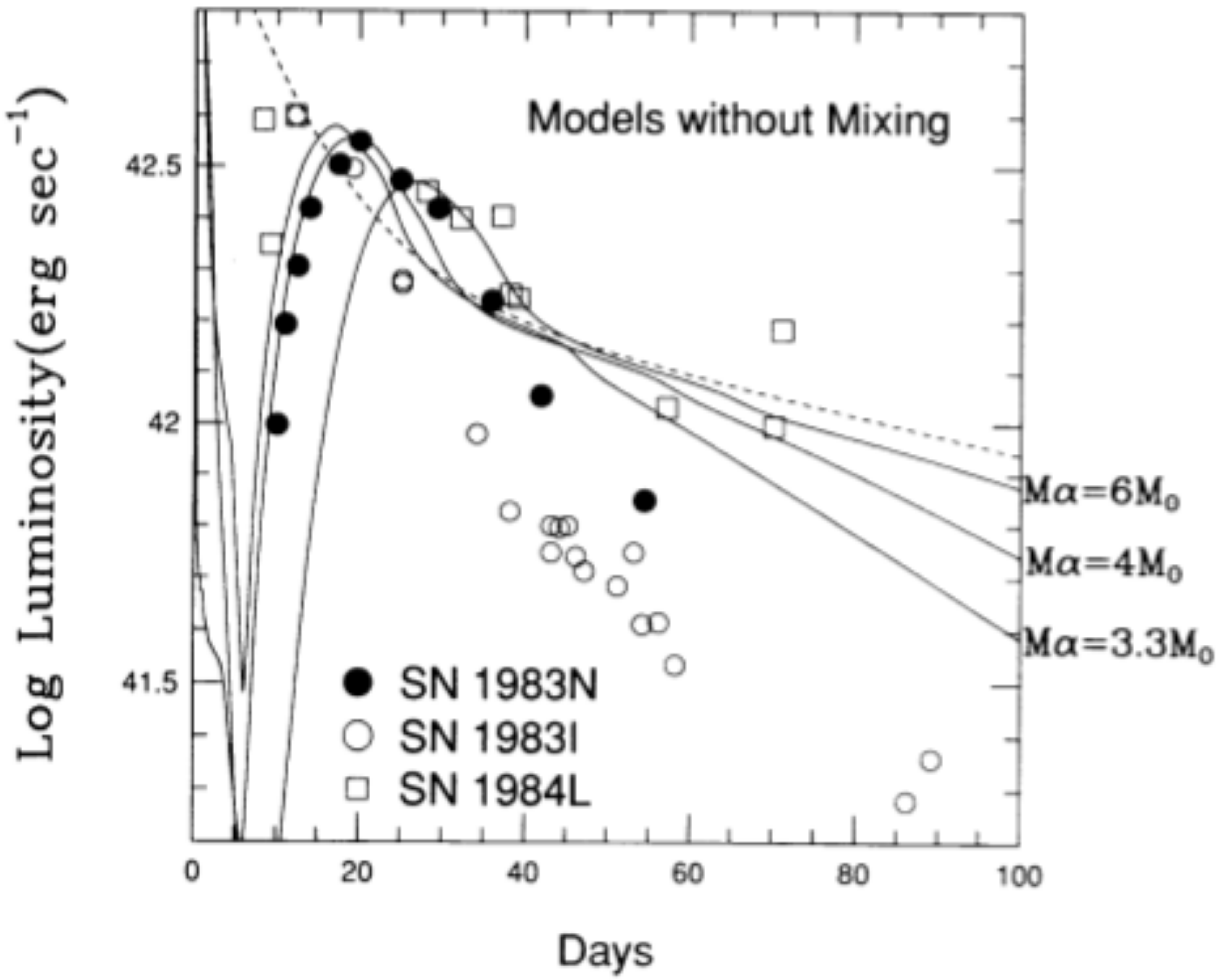

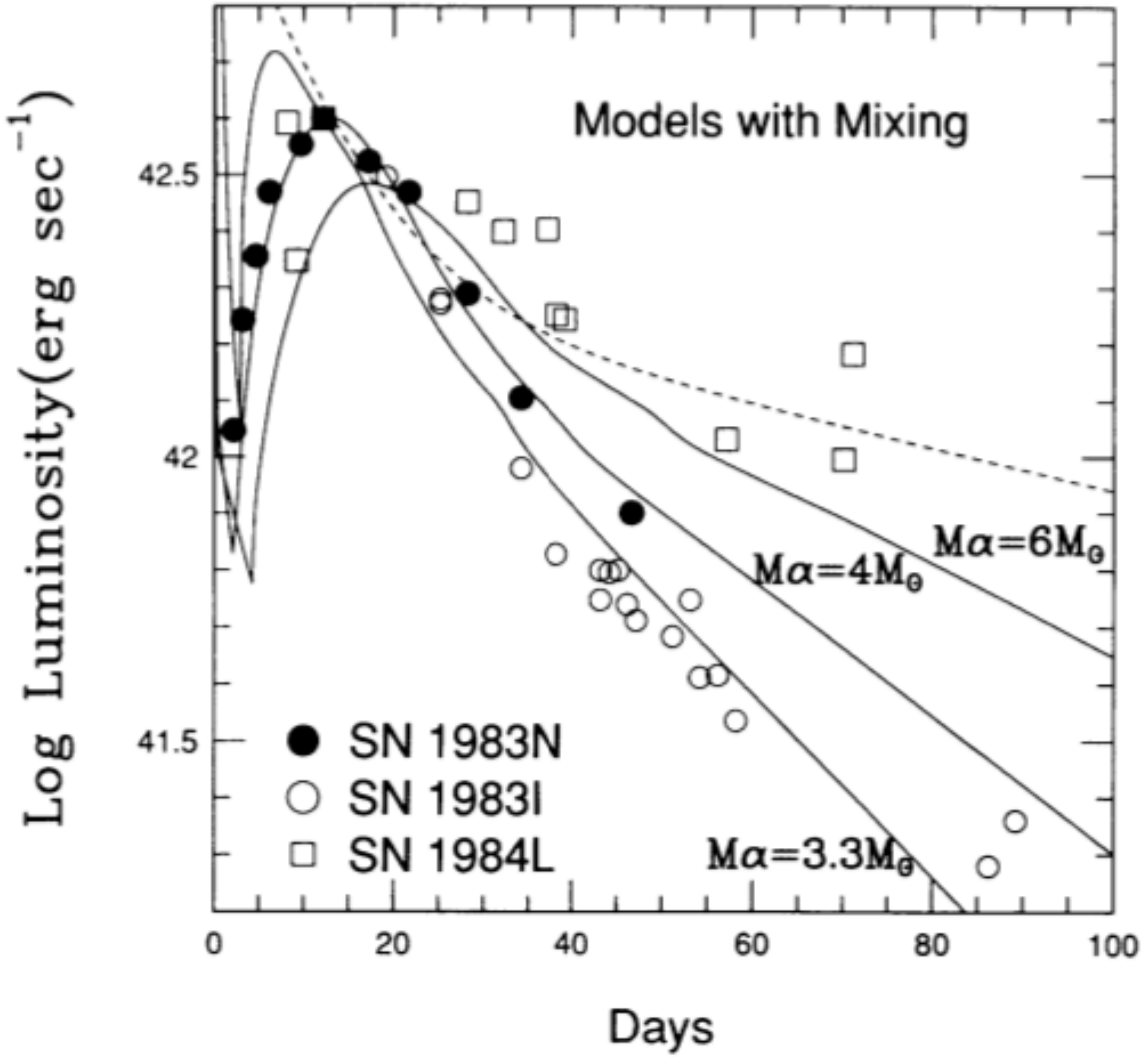

Shigeyama 1990.

Modelling SESN light curves

Very early observations (first days) can constrain the **progenitor radius**.
A SESN progenitor is always relatively compact ($R_0 \lesssim 200\ R_\odot$) so shock-deposited energy contributes only for $\lesssim$ few days because of adiabatic cooling ($E_{int} \propto R_0/R(t)$).

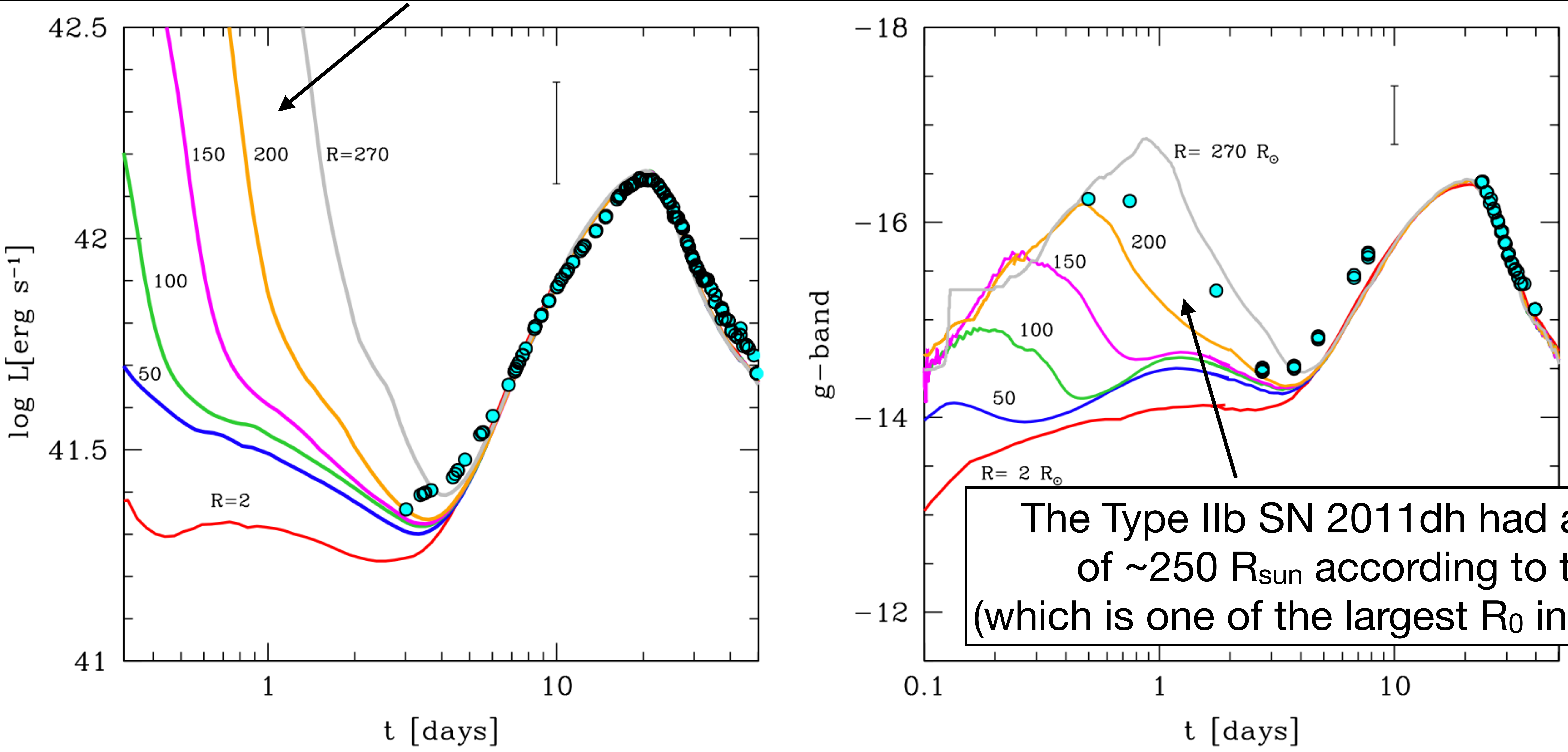

The Type IIb SN 2011dh had a progenitor radius of ~250 R_{sun} according to these model fits (which is one of the largest R_0 inferred for any SESN).

Bersten 2012

Figure 10. Bolometric LCs (left panel) and g'-band LCs (right panel) for models with the same explosion energy as our preferred model, but different initial radii. The observed bolometric LC (M. Ergon, in preparation) and g'-band LC (Arcavi et al. 2011) of SN 2011dh (cyan dots) are shown for comparison in each panel. The error bars indicate the size of the systematic uncertainty that corresponds to an uncertainty of 1 Mpc in the distance to M51. The radius variation is accomplished by attaching essentially massless ($<0.01\ M_\odot$) envelopes to the He4 model. Larger radii produce higher early luminosity for $t \lesssim 5$ days but no appreciable effect is seen at later times.

Direct progenitor detections of SESNe confirm more compact stars than RSGs

So far 5 Type IIb SNe
and 2 Type Ib SNe (iPTF13bvn and 2019yvr)

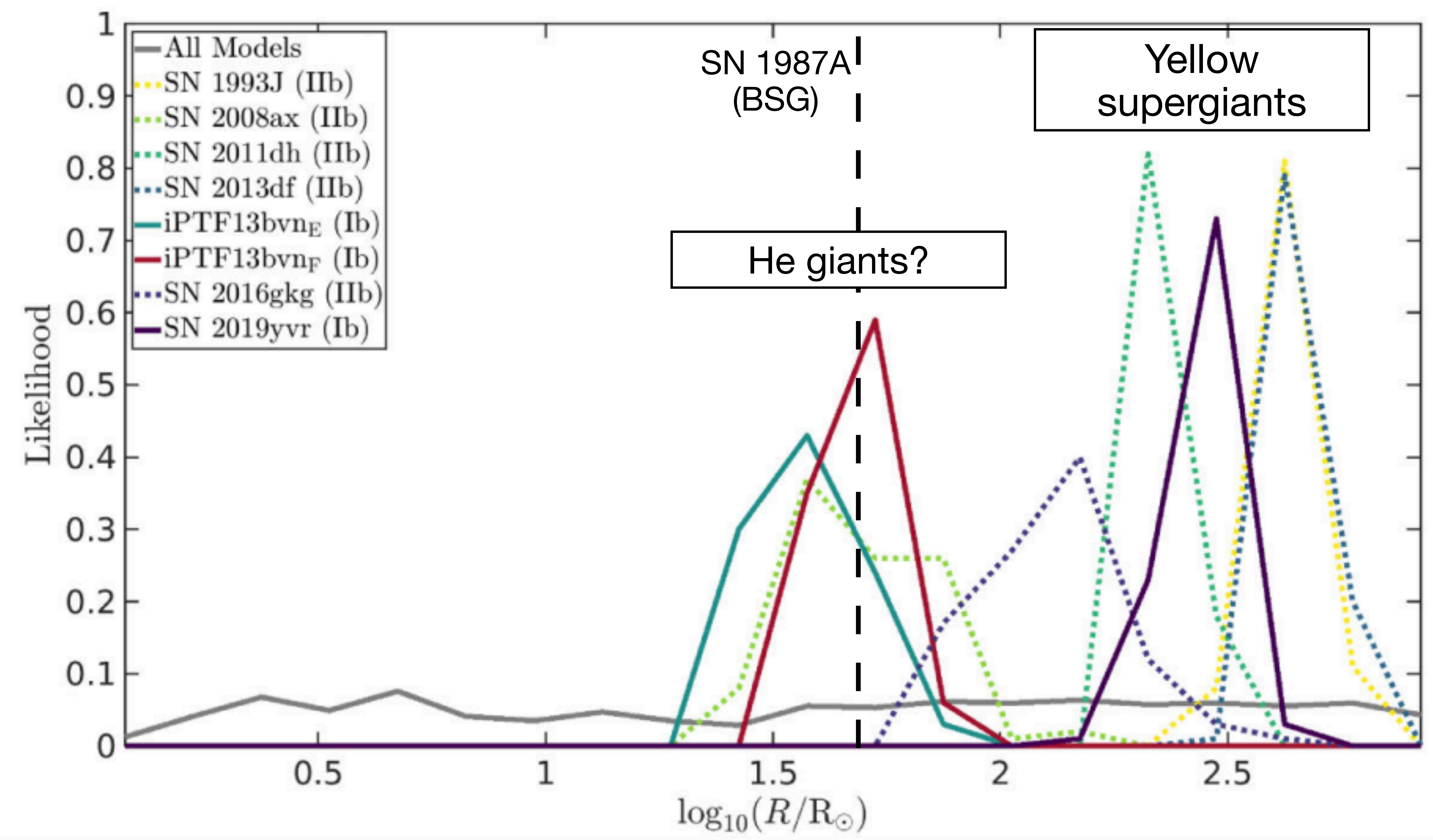

Gilkis 2022

Direct progenitor detections of SESNe

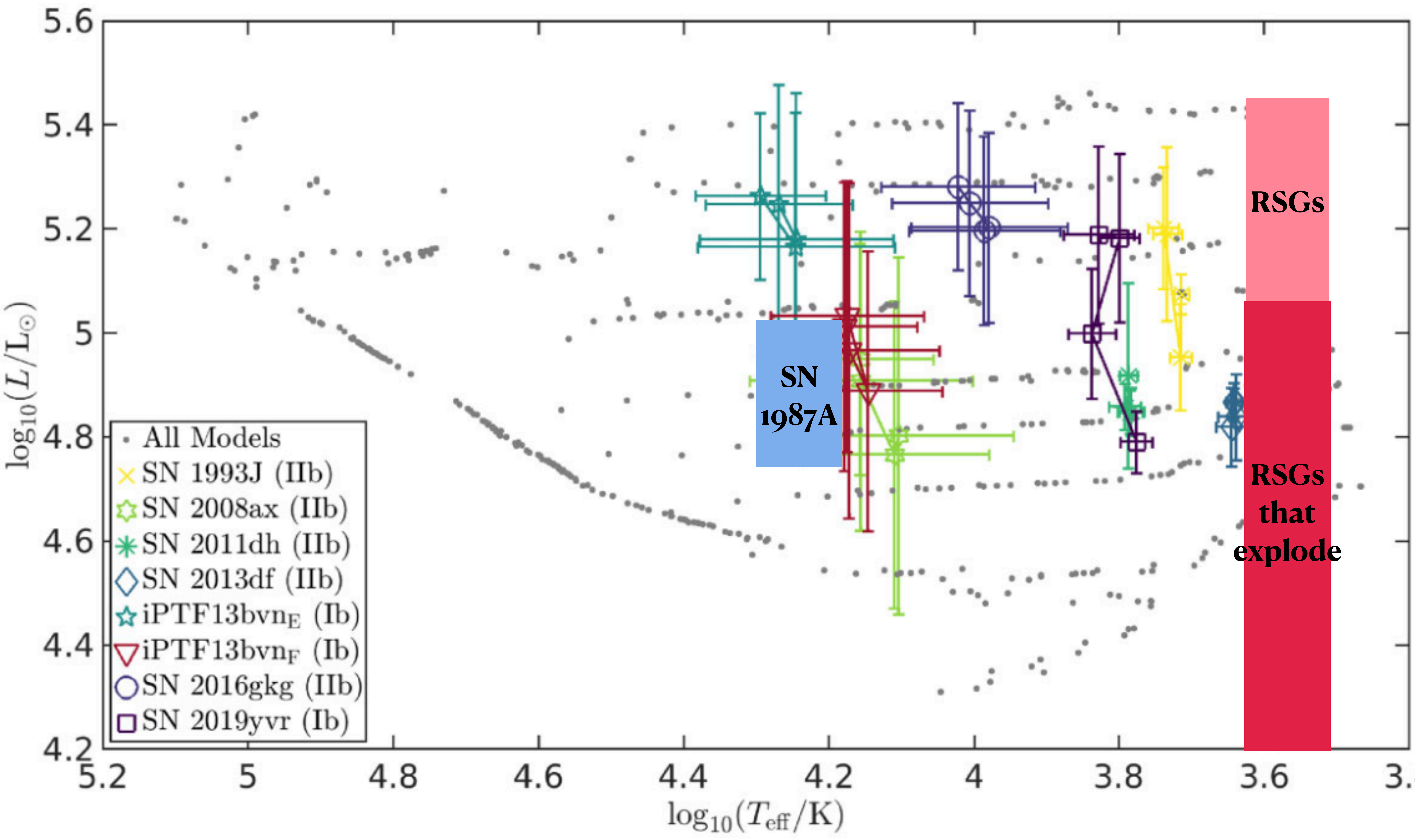

Gilkis 2022

Binary mass transfer appears most plausible explanation for progenitors

iPTF13bvn : a typical binary model progenitor system:

Exploding star a M_{ZAMS}=10-12 Msun star ending as a **2-3 M_{sun} He giant** after mass transfer to a companion star.

Table 2. Physical parameters of the binary progenitor models which match the observed constraints on the progenitor of iPTF13bvn.

Primary parameter	Value	Secondary parameter	Value
$M_{1,i}/M_\odot$	11.0 ± 1.2	$M_{2,i}/M_\odot$	5.8 ± 2.9
$M_{1,f} M_\odot$	2.4 ± 0.4	$M_{2,f}/M_\odot$	5.0 ± 4.5
$\log(L_1/L_\odot)$	4.6 ± 0.1	$\log(L_2/L_\odot)$	1.1 ± 2.9
$\log(T_{1,\rm eff}/K)$	4.06 ± 0.04	$\log(T_{2,\rm eff}/K)$	4.0 ± 0.4
$\log(R_1/R_\odot)$	1.71 ± 0.04	$\log(R_2/R_\odot)$	0.4 ± 0.3
$M_{\rm ejecta} M_\odot$	0.95 ± 0.4		
$M_{\rm He} M_\odot$	0.6 ± 0.2		
	System parameters		
$\log(P_i/\rm d)$	1.9 ± 0.5	$\log(a_f/R_\odot)$	1.8 ± 0.2
Age/Myr	24 ± 5	Z	0.027 ± 0.013

Companion a low-mass, dim star.

Eldridge & Maund 2016

Modelling SESN light curves

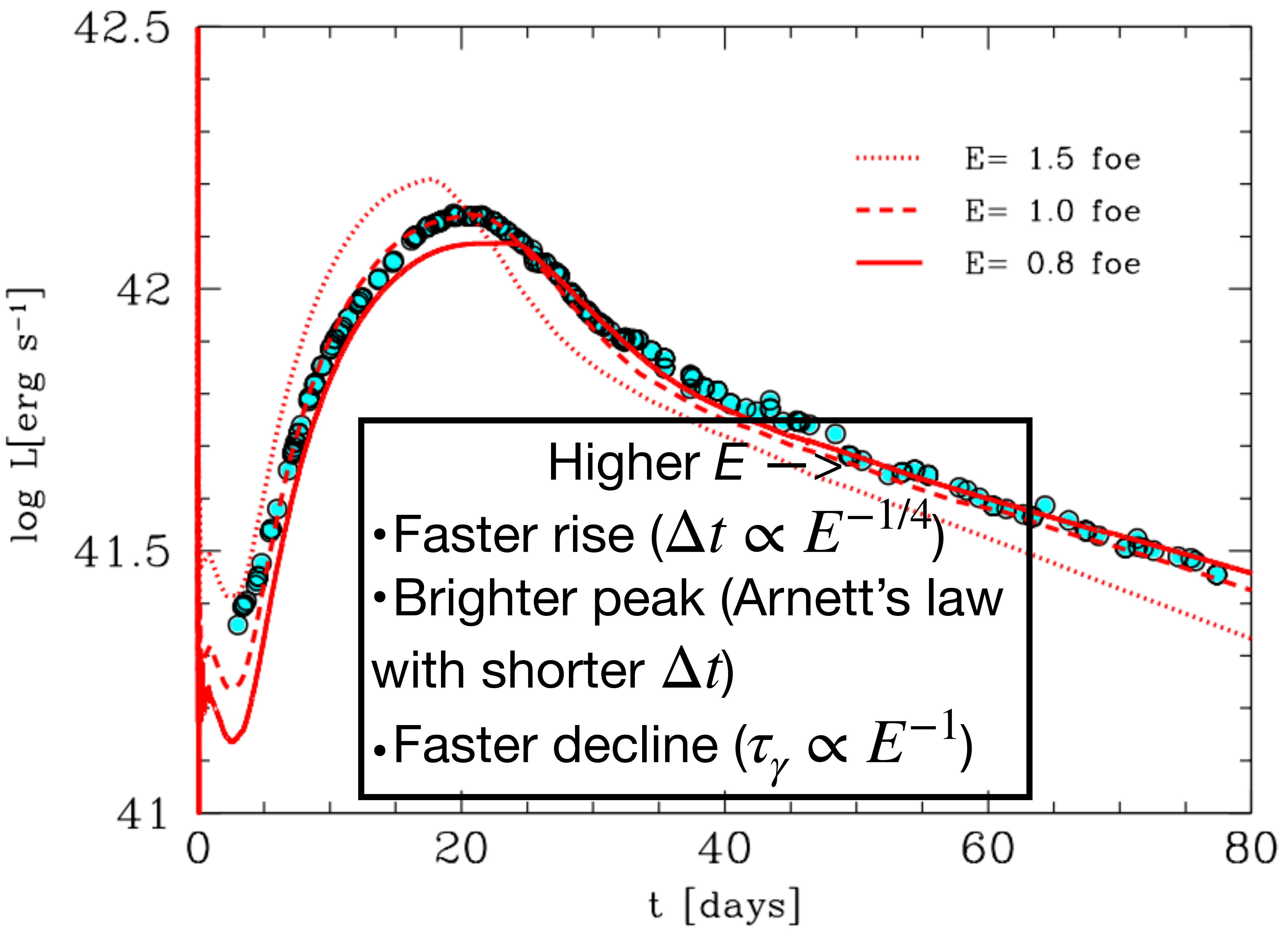

Figure 2. Sensitivity of the bolometric LC to changes in the explosion energy. The He4 initial model (see Section 3.1) and three different values of the explosion energy, E = 0.8, 1.0, 1.5 foe, were used in these simulations. The observed bolometric LC of SN 2011dh (points) is shown for comparison.

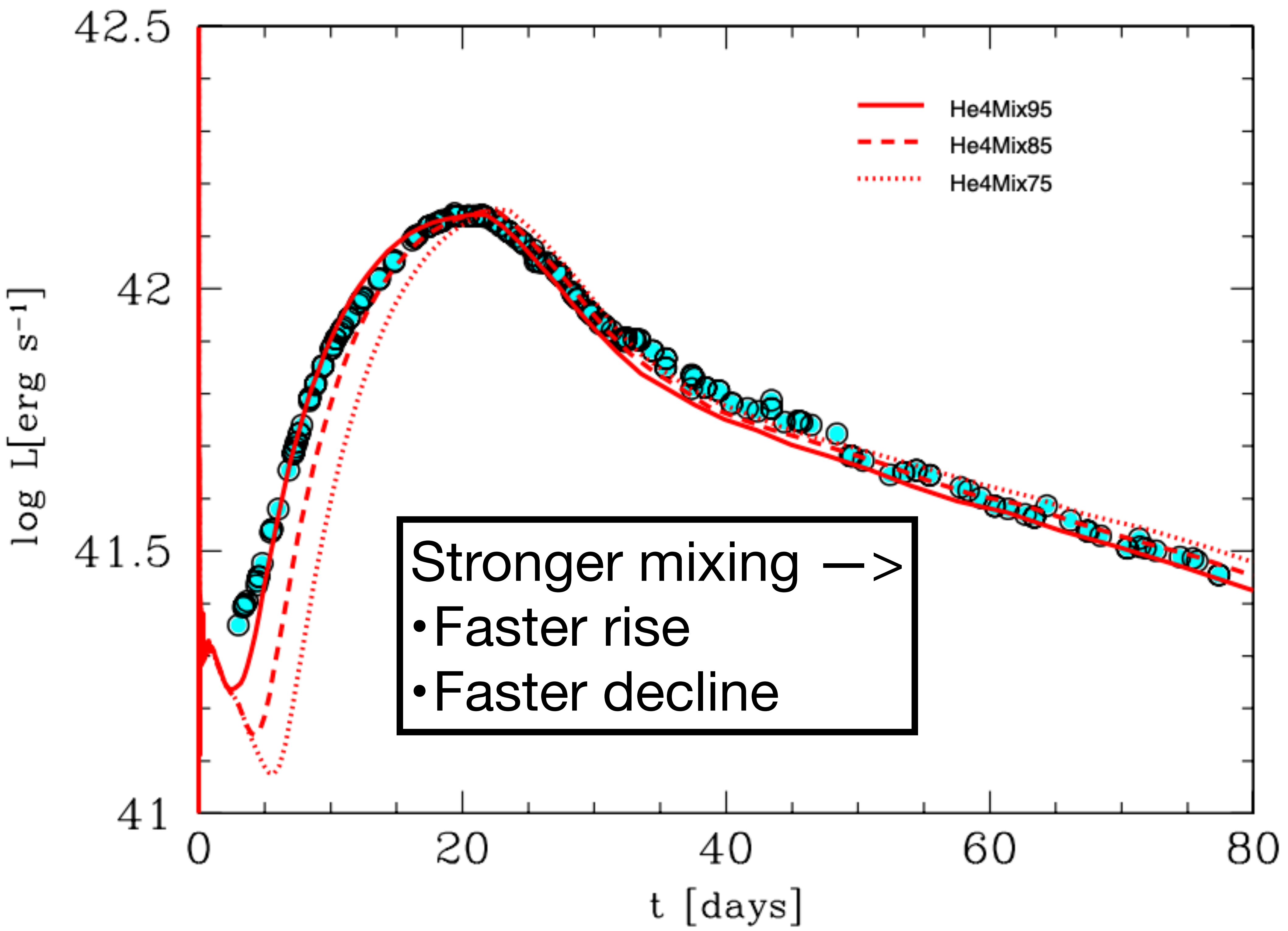

Figure 5. Sensitivity of the bolometric LC to changes in the ^{56}Ni distribution. The He4 initial model with ^{56}Ni mass = 0.06 $M_\odot$ (see Section 3.1) and three different degrees of mixing, up to 75% (He4Mix75), 85% (He4Mix85), and 95% (He4Mix95) of the total initial mass, were used in these simulations. The observed bolometric LC of SN 2011dh (points) is shown for comparison.

Bersten 2012

Modelling SESN light curves

Dessart 2016

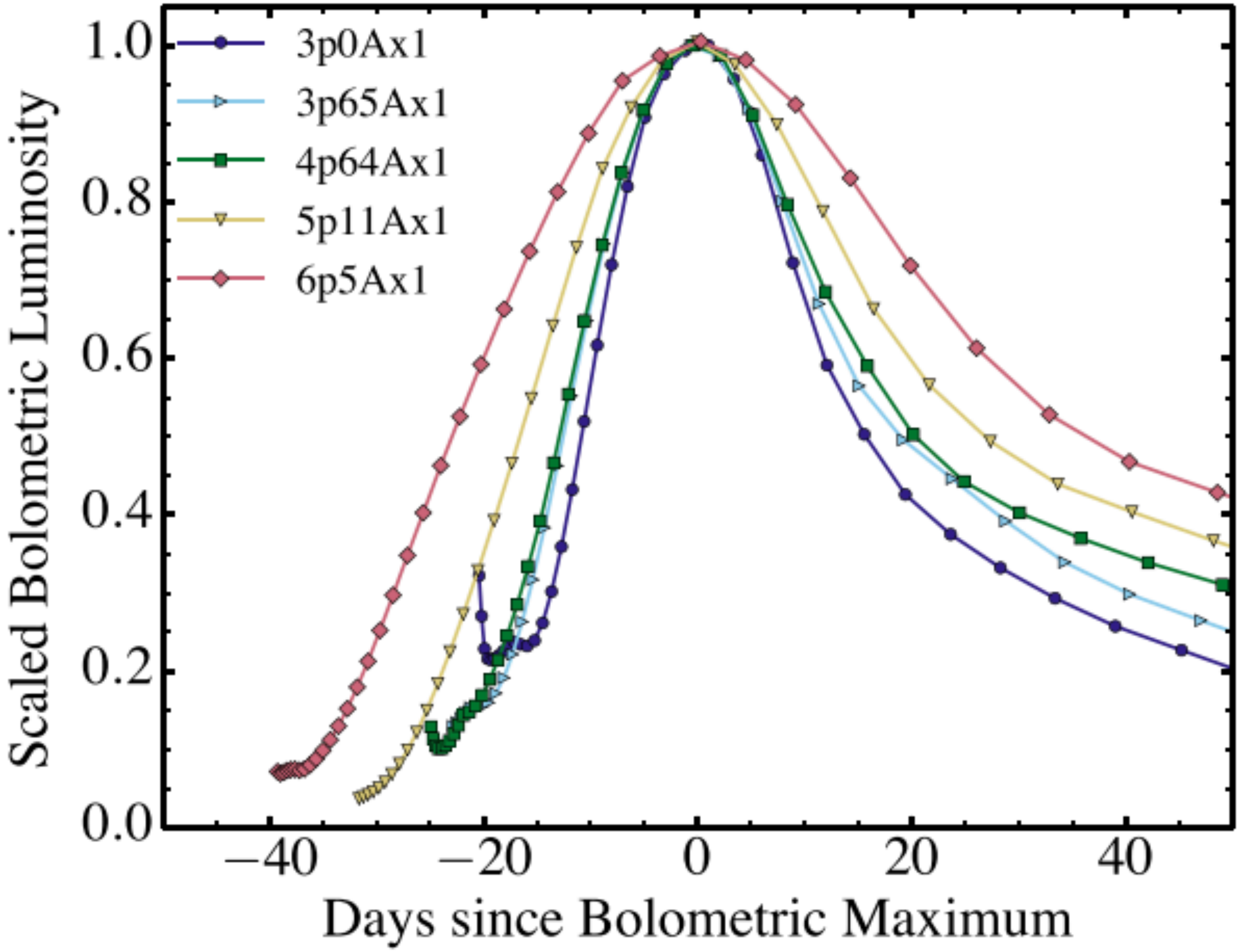

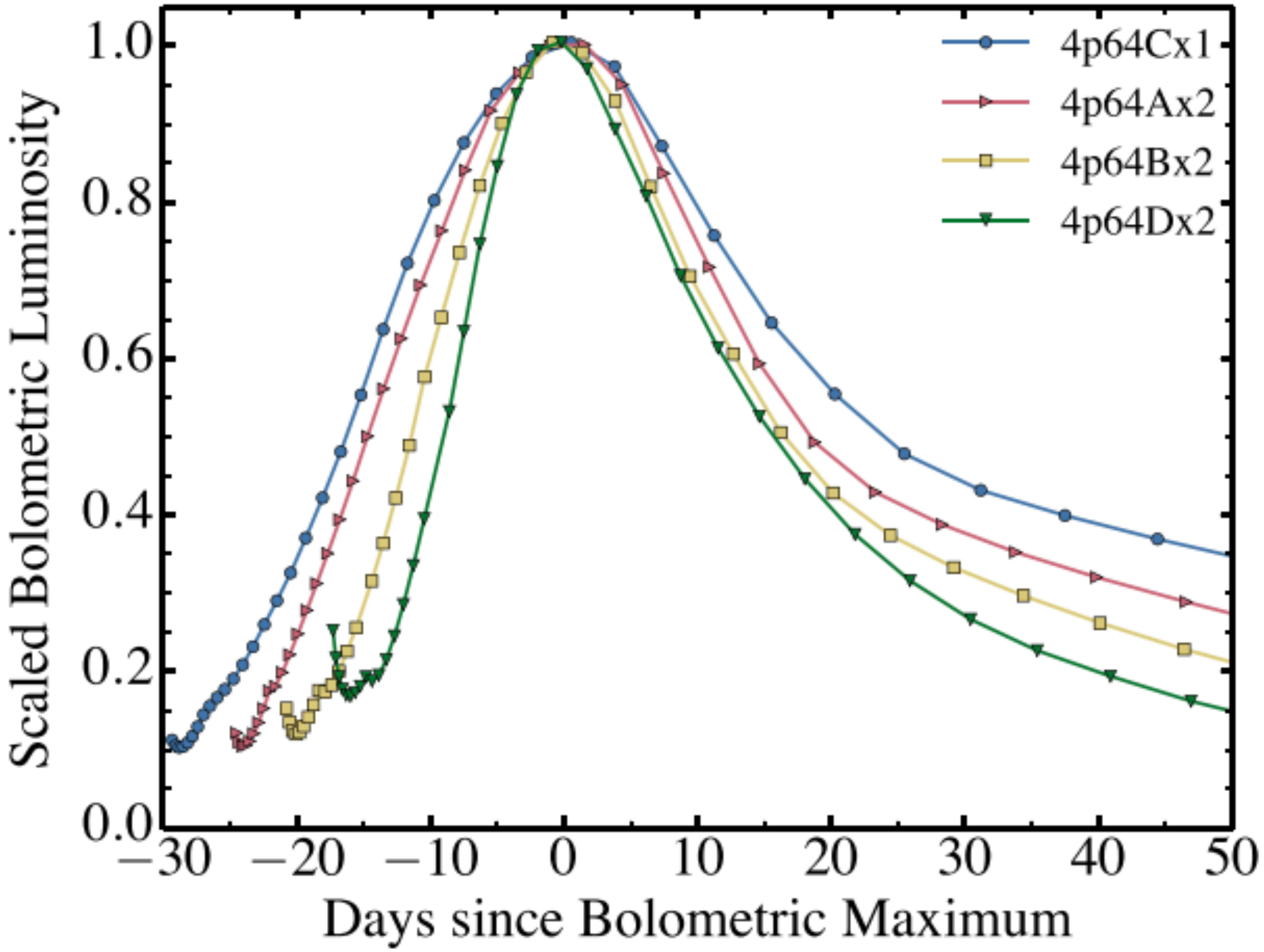

For fixed E, and (quasi)-fixed ^{56}Ni mass, **higher ejecta mass means broader light curves**. Here range is 1.7-5.0 M_{sun}.

For fixed M, and (quasi)-fixed ^{56}Ni mass, **higher explosion energy means narrower light curves**. Here range is 0.6-5 Bethe (C→D).

Testing analytic approximations against detailed numeric models

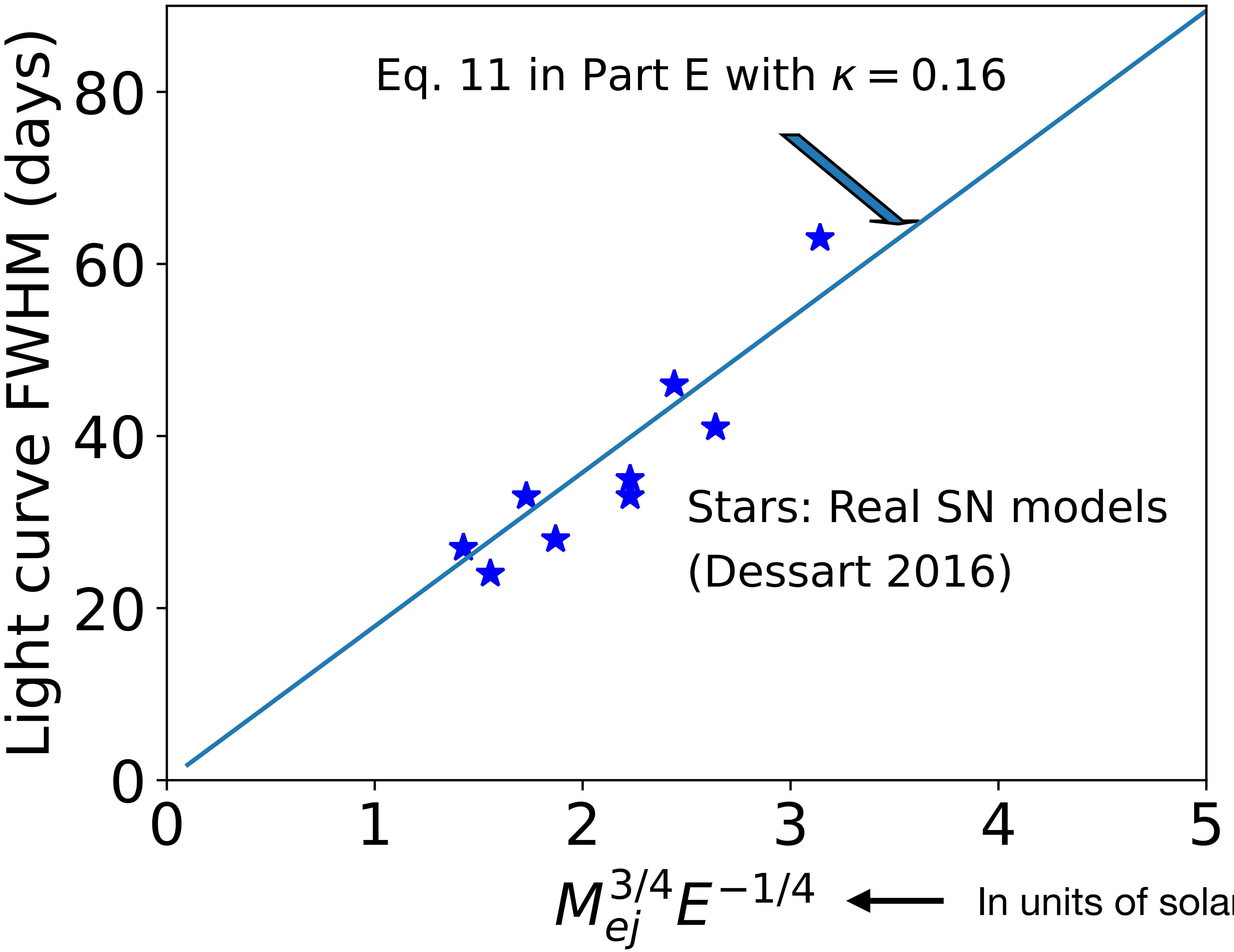

← In units of solar masses and 1E51 erg

Testing Arnett’s law

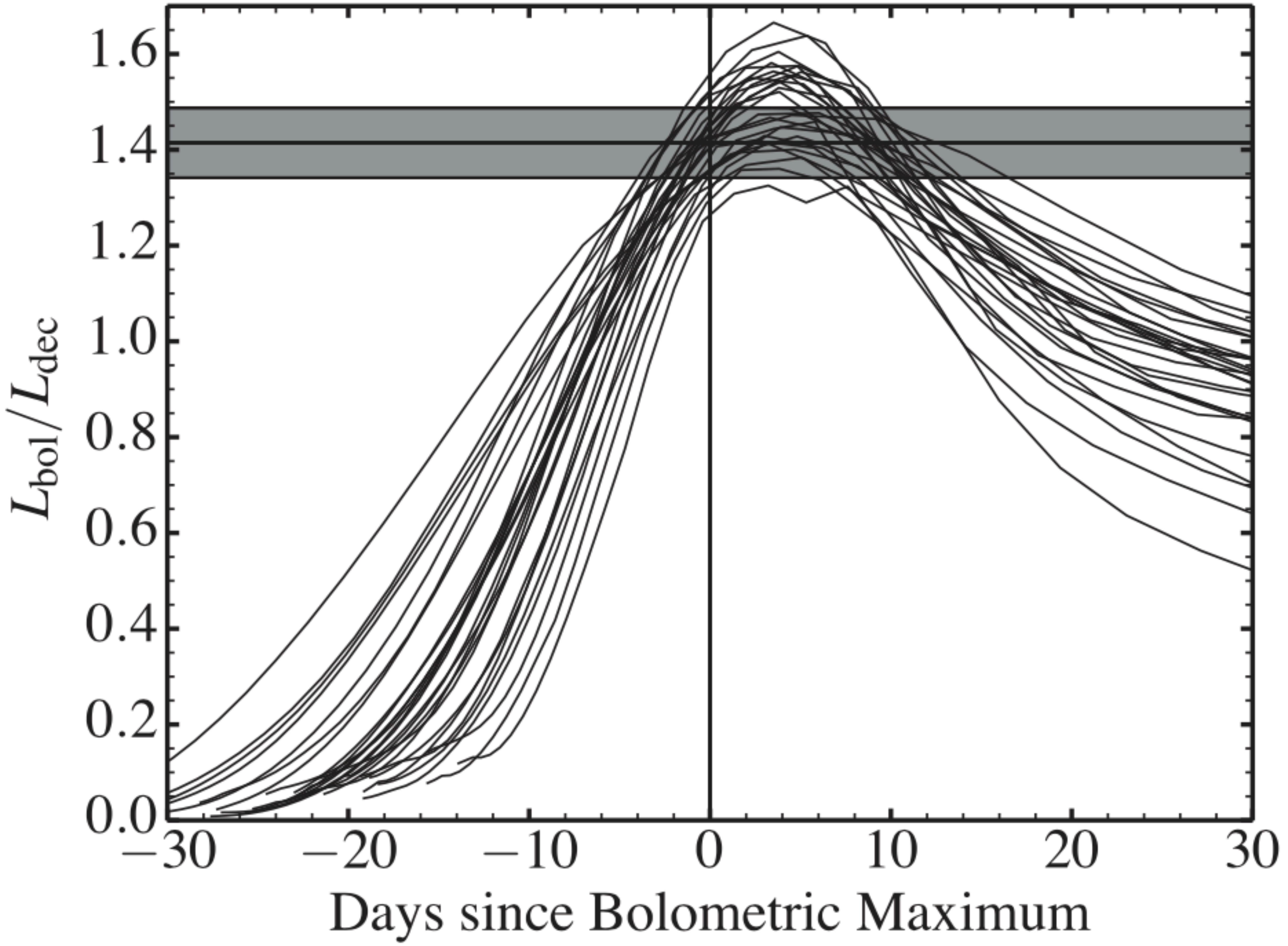

Figure 18. Variation of the ratio $L_{\rm bol}/L_{\rm dec}$ versus time since bolometric maximum for our grid of SNe IIb/Ib/Ic models. The ratio at bolometric maximum has a mean of 1.41 and a standard deviation of σ =0.072. The shaded area corresponds to the mean $\pm\sigma$.

Arnett's law ($L(t_{peak}) = S(t_{peak})$) can be compared to advanced light curve models.

This particular model grid indicates that the ^{56}Ni mass inferred by Arnett’s law is 30-60% too high.

This is important to be aware of because sample analyses tend to use simple analytic models like Arnett’s - and there can be systematic errors.

Dessart 2016

Modelling SESN photospheric spectra

SYNOW/SYN++ : Parameterise abundances in scattering atmosphere ansatz and fit. Useful to identify lines. Another, more sophisticated code, is **TARDIS**.

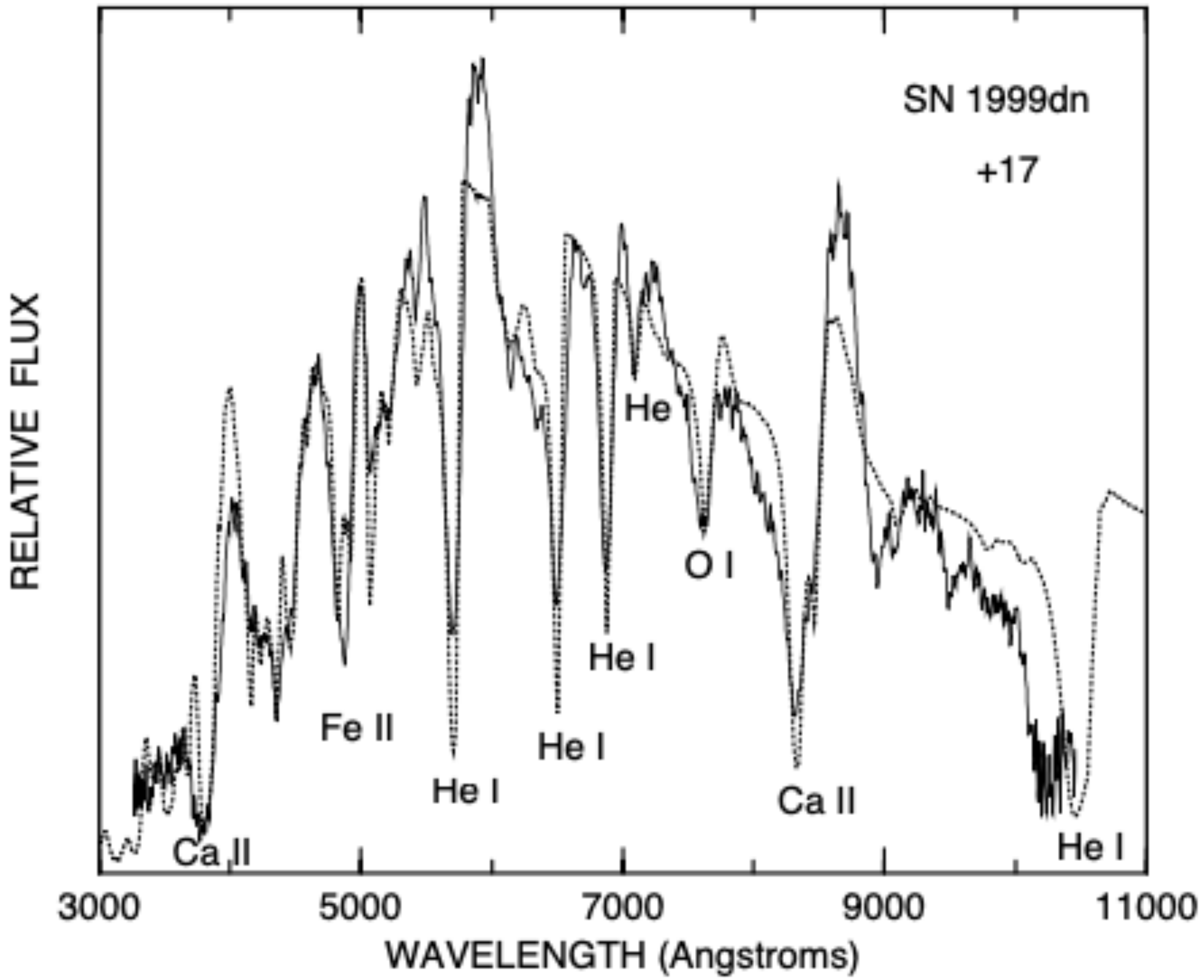

Branch 2002

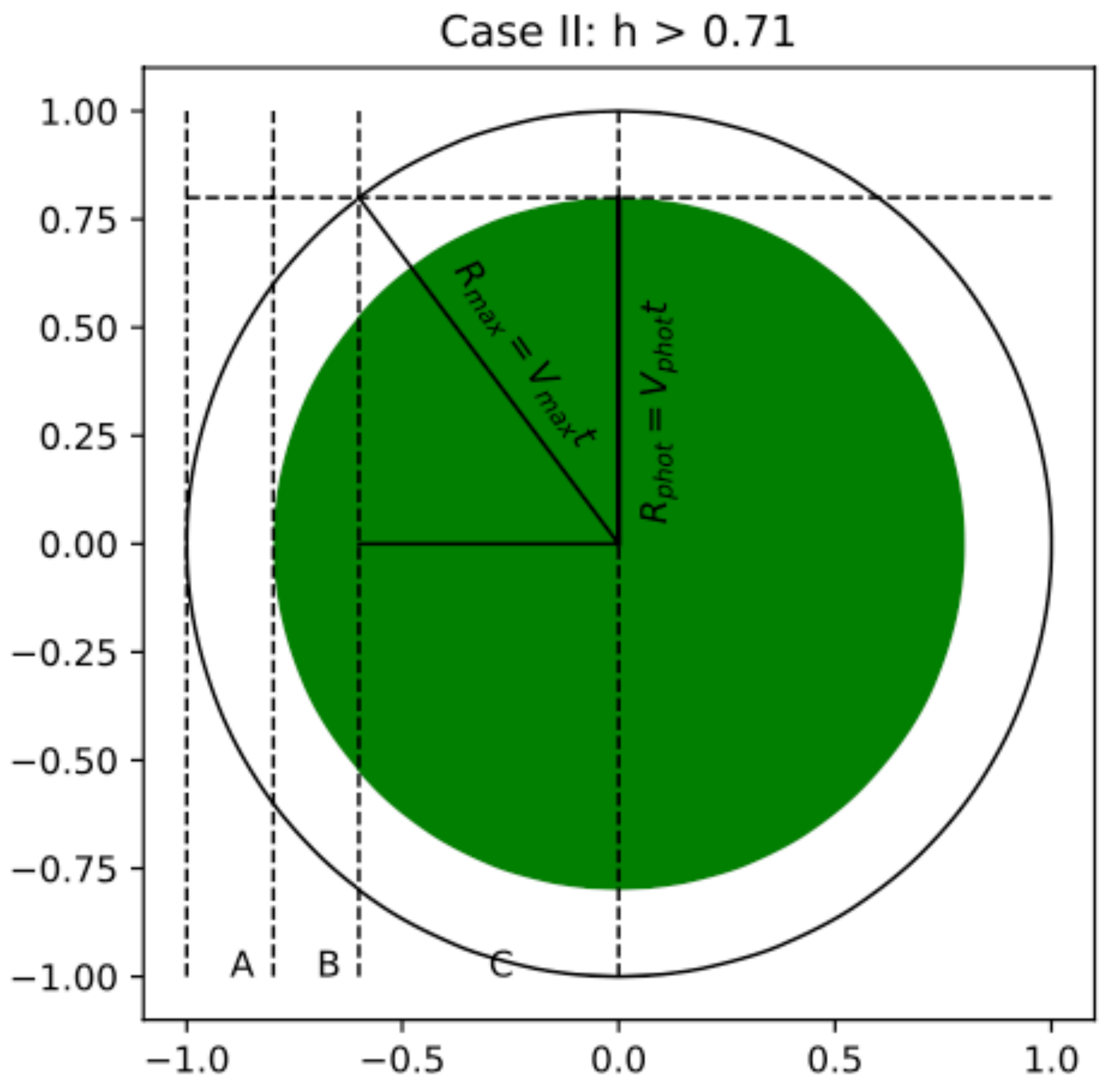

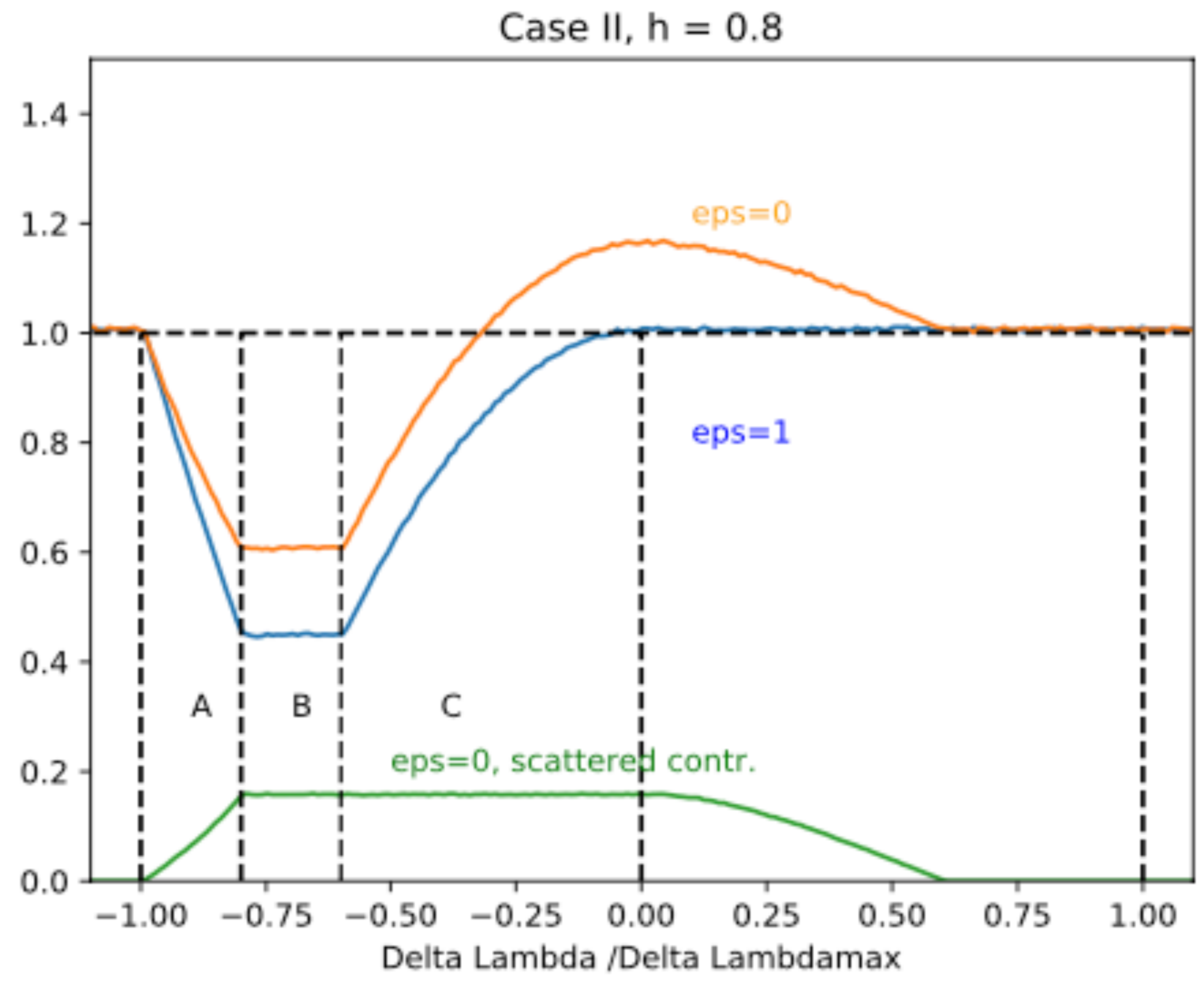

Modelling SESN photospheric spectra

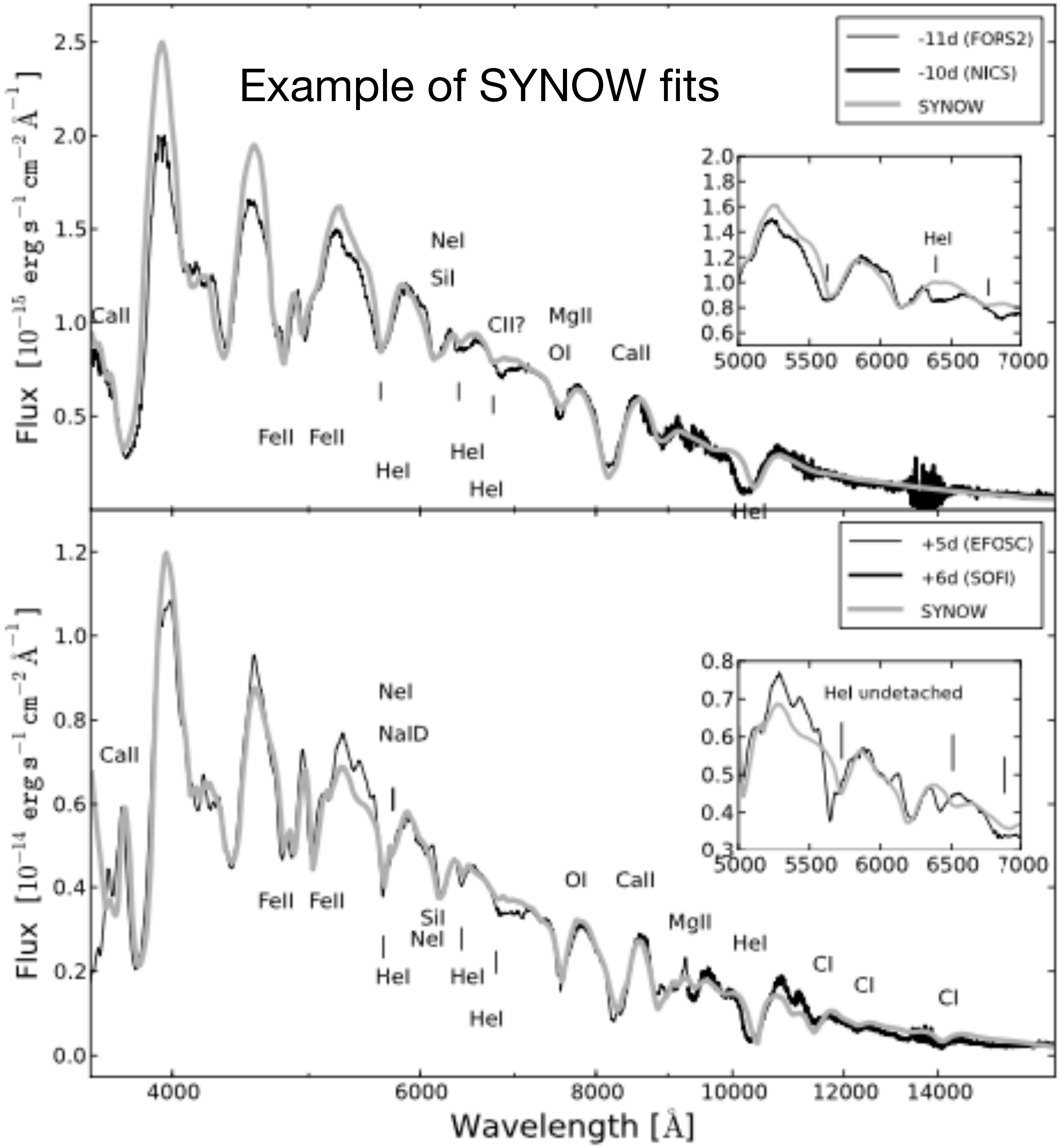

Valenti 2011

Are Ic SNe really He free or just He-*emission* free?

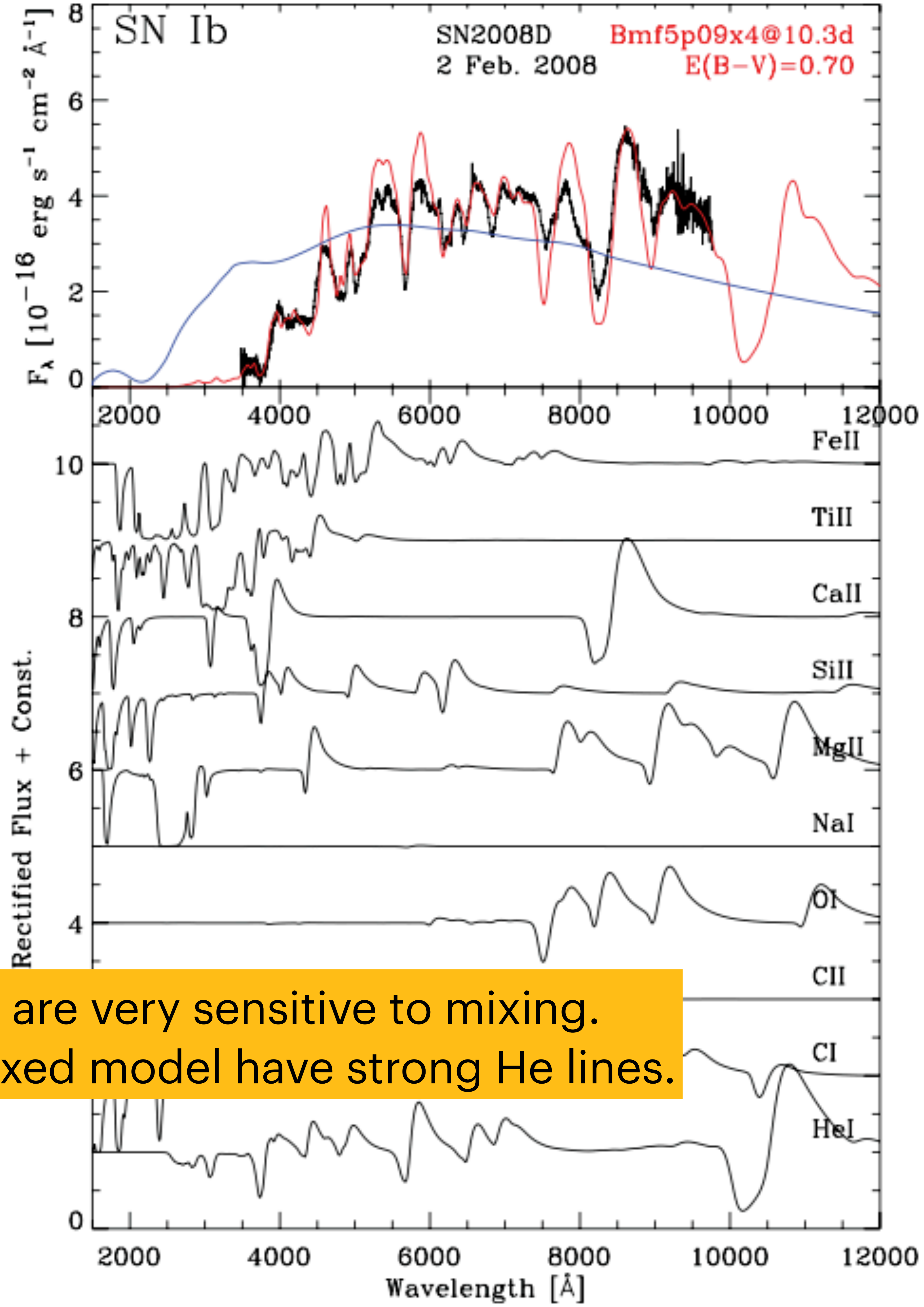

He lines are very sensitive to mixing.
Strongly mixed model have strong He lines.

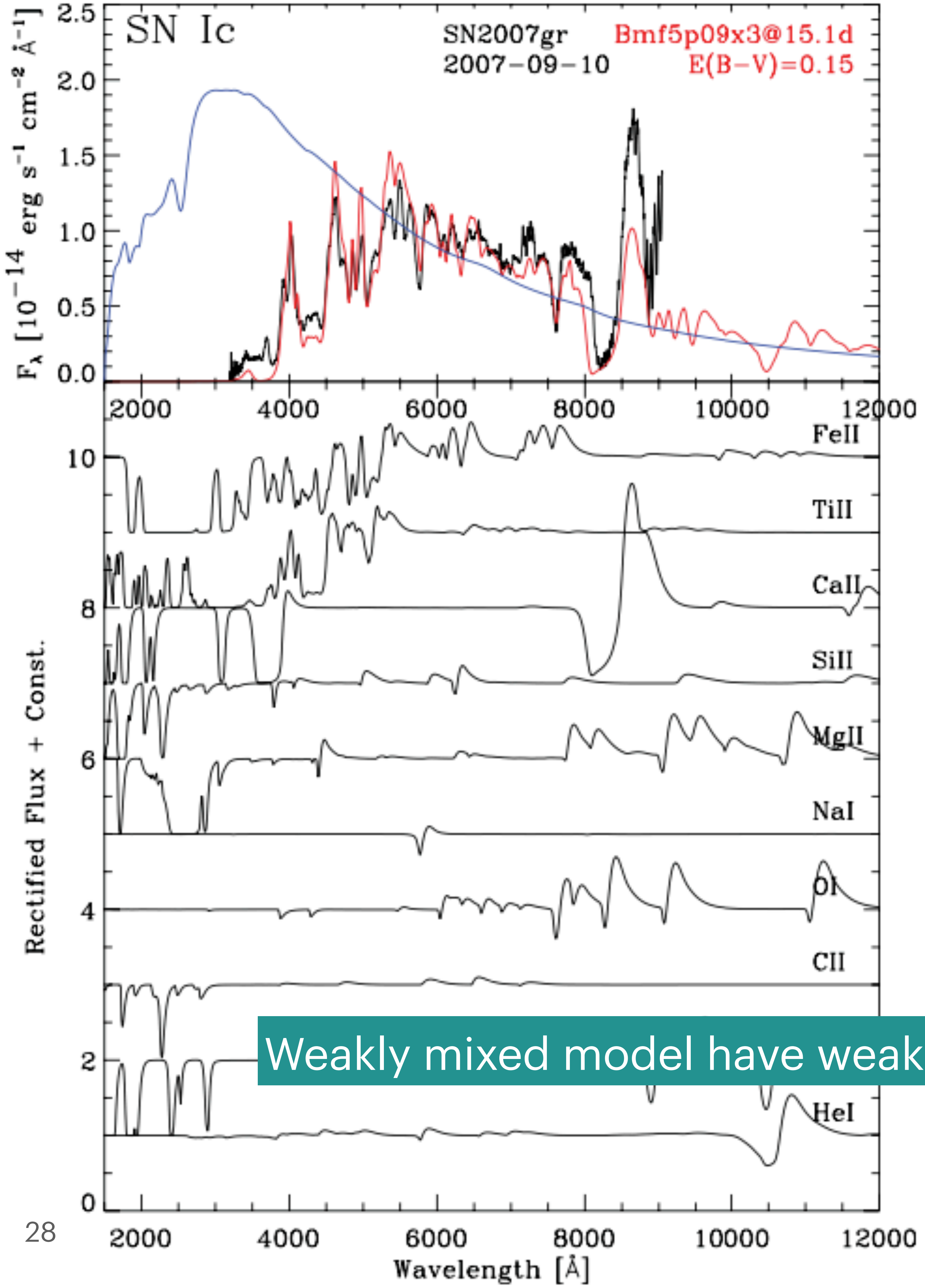

Weakly mixed model have weak He lines.

Dessart 2012

SESN nebular spectra

Stritzinger 2009

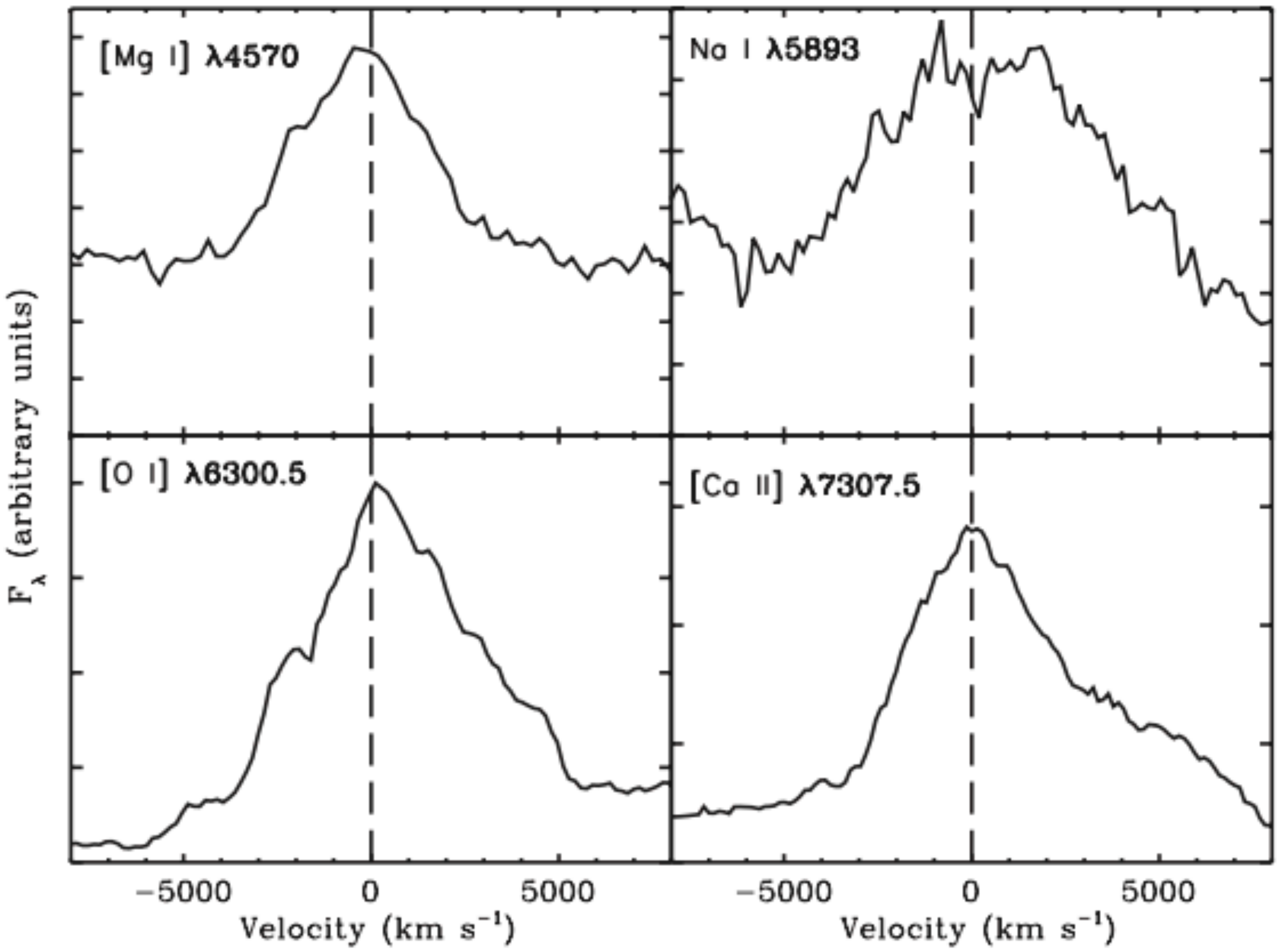

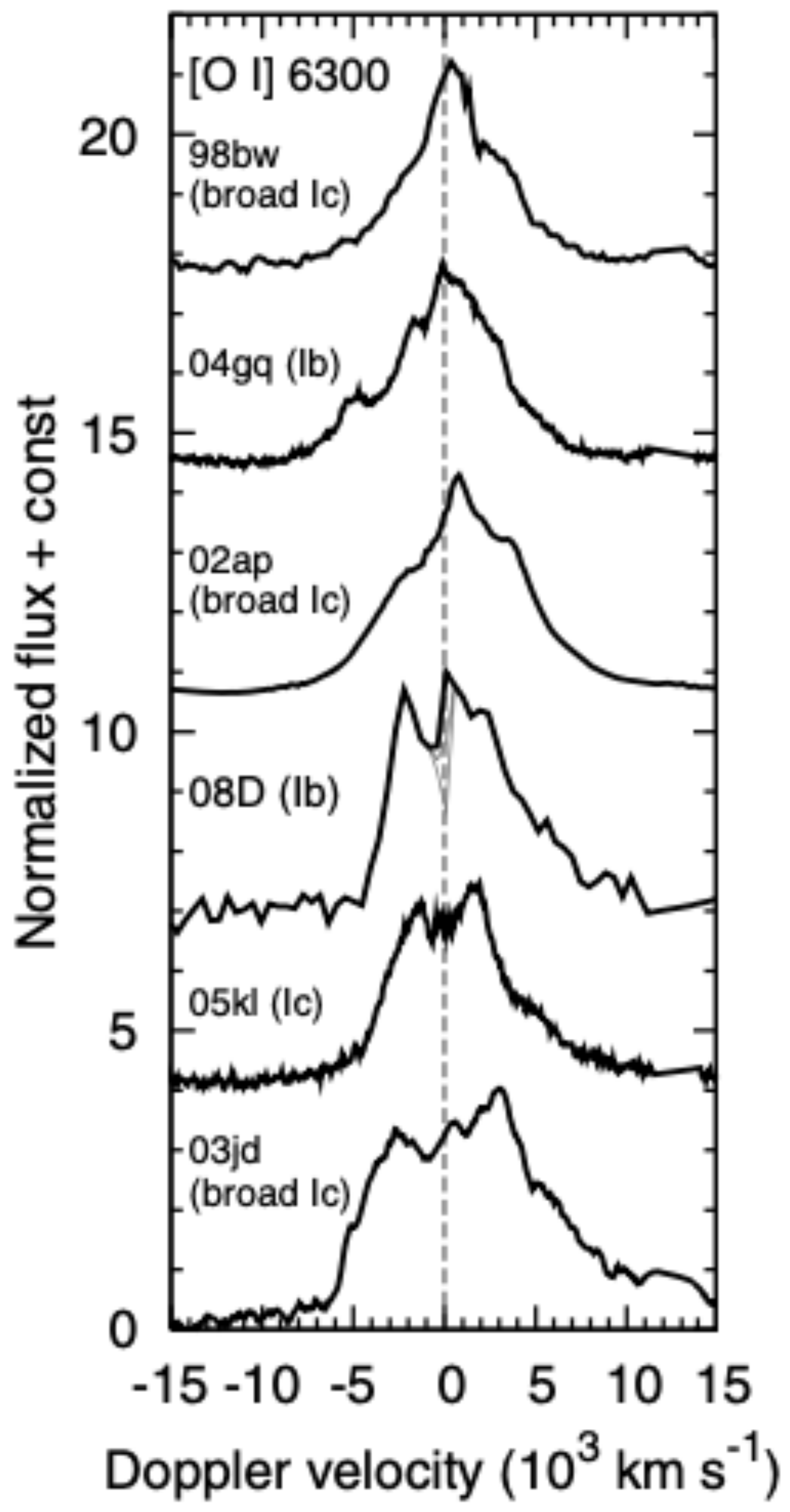

Tanaka 2009

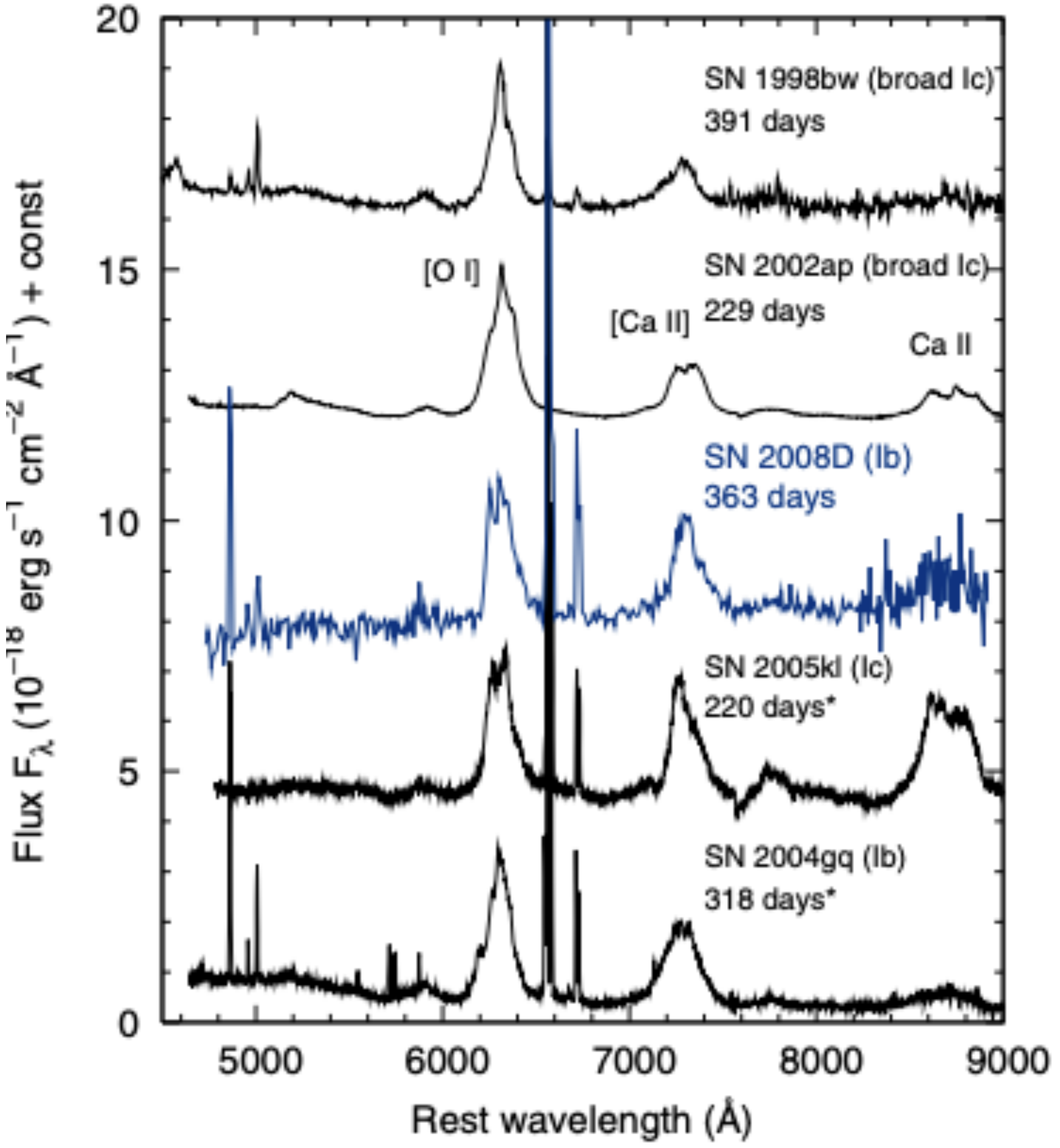

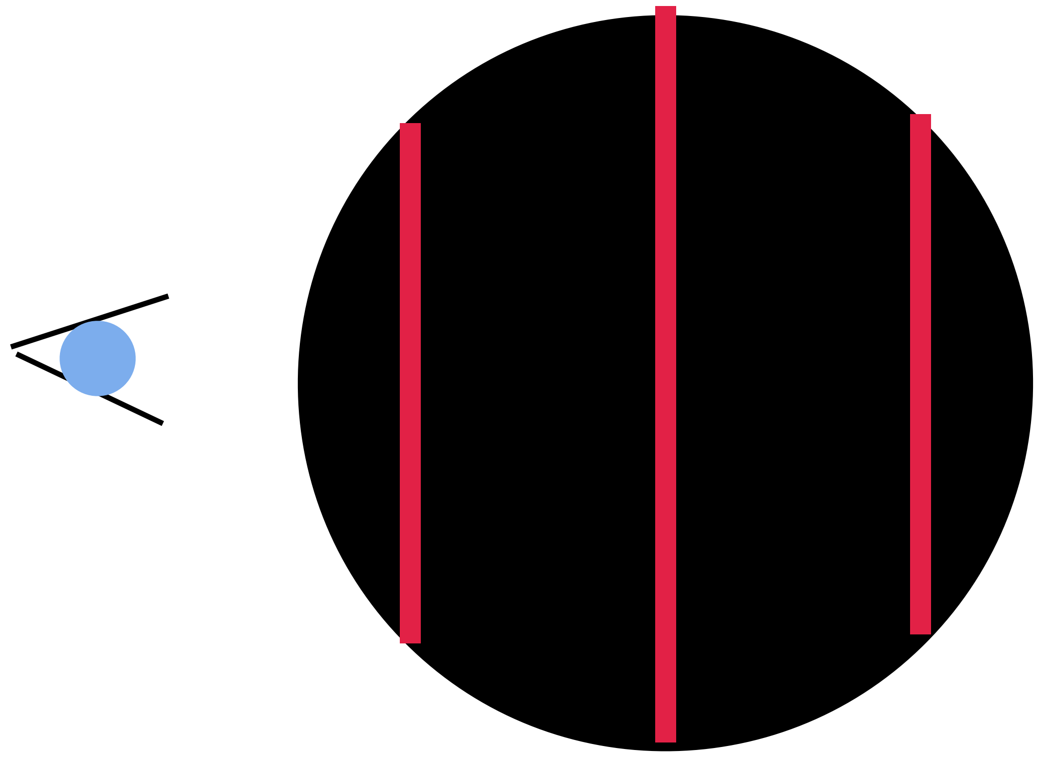

The sheet's area determines the flux at the corresponding Doppler shift.

Uniform sphere —> parabolic line profile.

Observed v_{max} —> **Metal core expands with char. velocity 4000 km/s.**

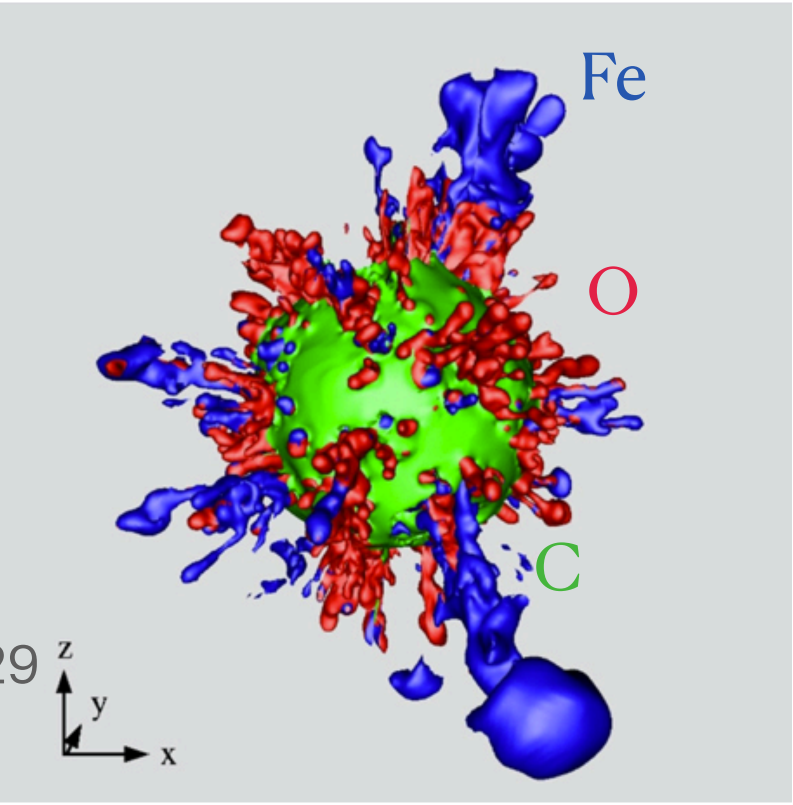

Line profile details depend on the 3D morphology of the inner ejecta —> **probe of explosion dynamics.**

Modelling SESN nebular spectra

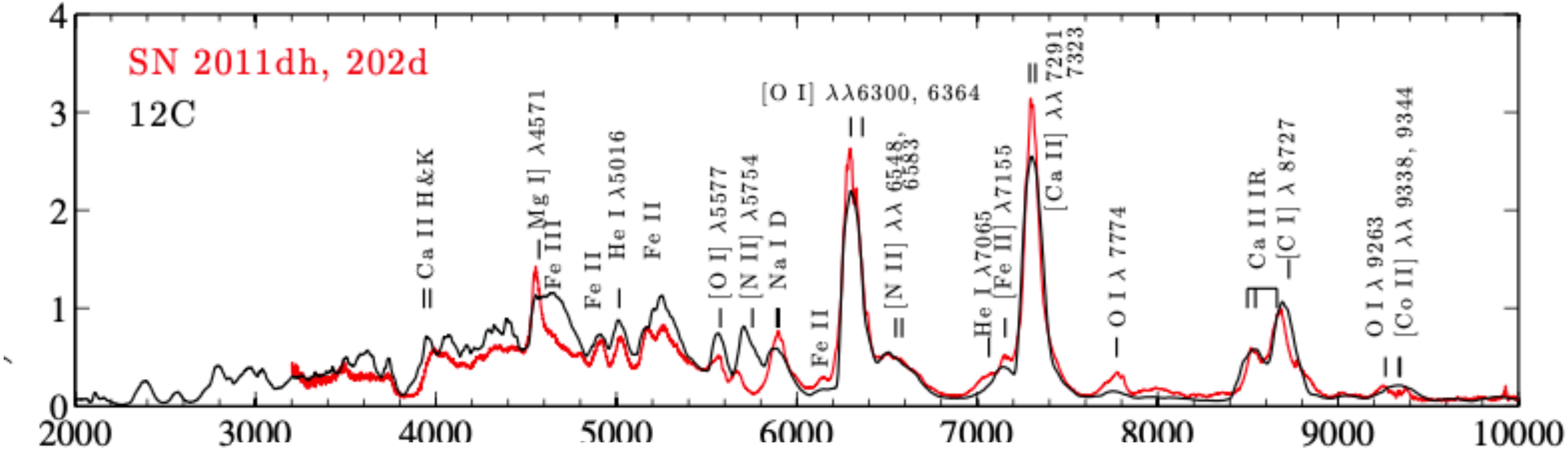

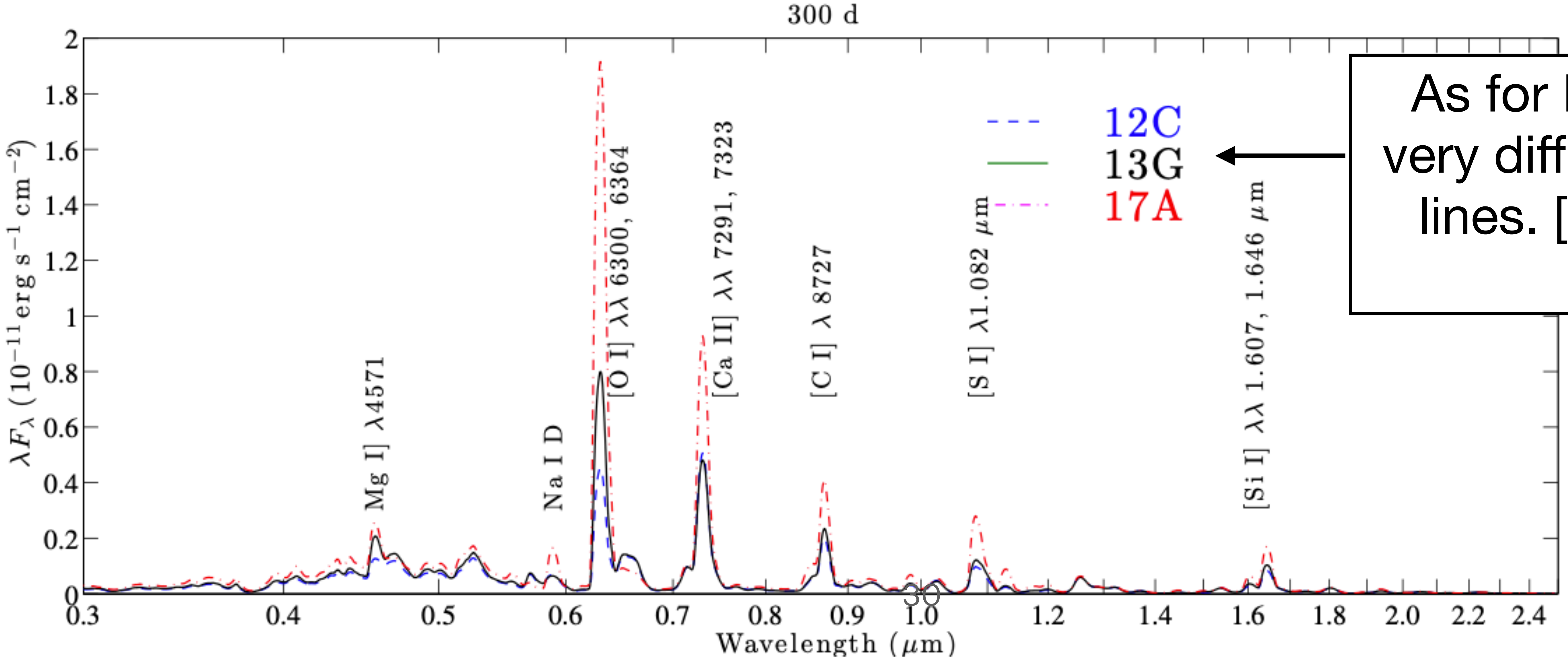

As for H-rich SNe, varying M_{ZAMS} gives very different length strengths for certain lines. [O I] 6300, 6364 is best probe of M_{ZAMS}.

Jerkstrand 2015

Modelling SESN nebular spectra

Luminosity in [O I] 6300, 6364 relative to ^{56}Co decay power.

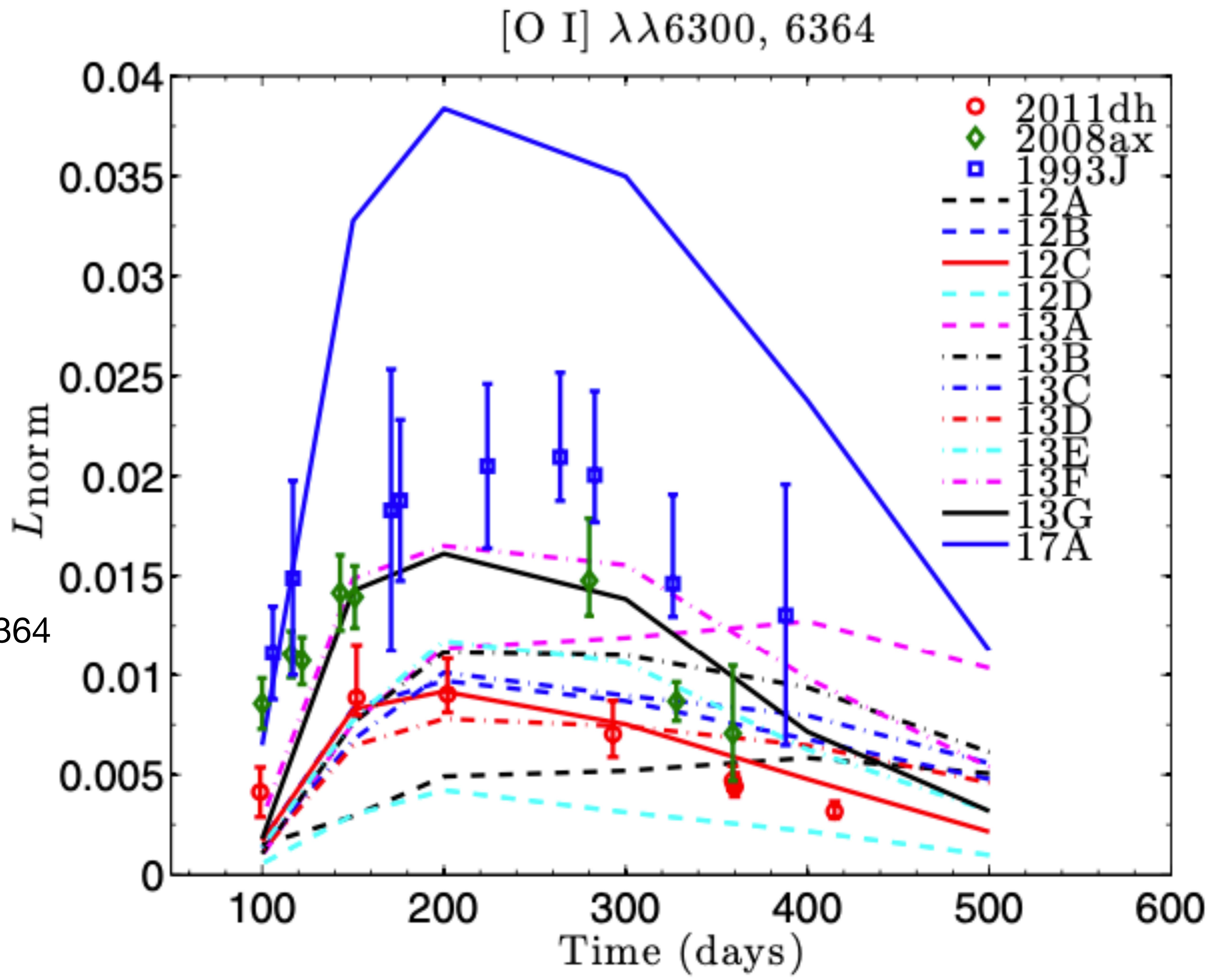

As Type IIP SNe, stripped-envelope SNe appear to have nucleosynthesis yields consistent with lower-mass stars (M_{ZAMS} <~ 20 M_{sun}).

Jerkstrand 2015

Modelling SESN nebular spectra

Models allow to determine **which stellar burning layer** each line diagnoses.

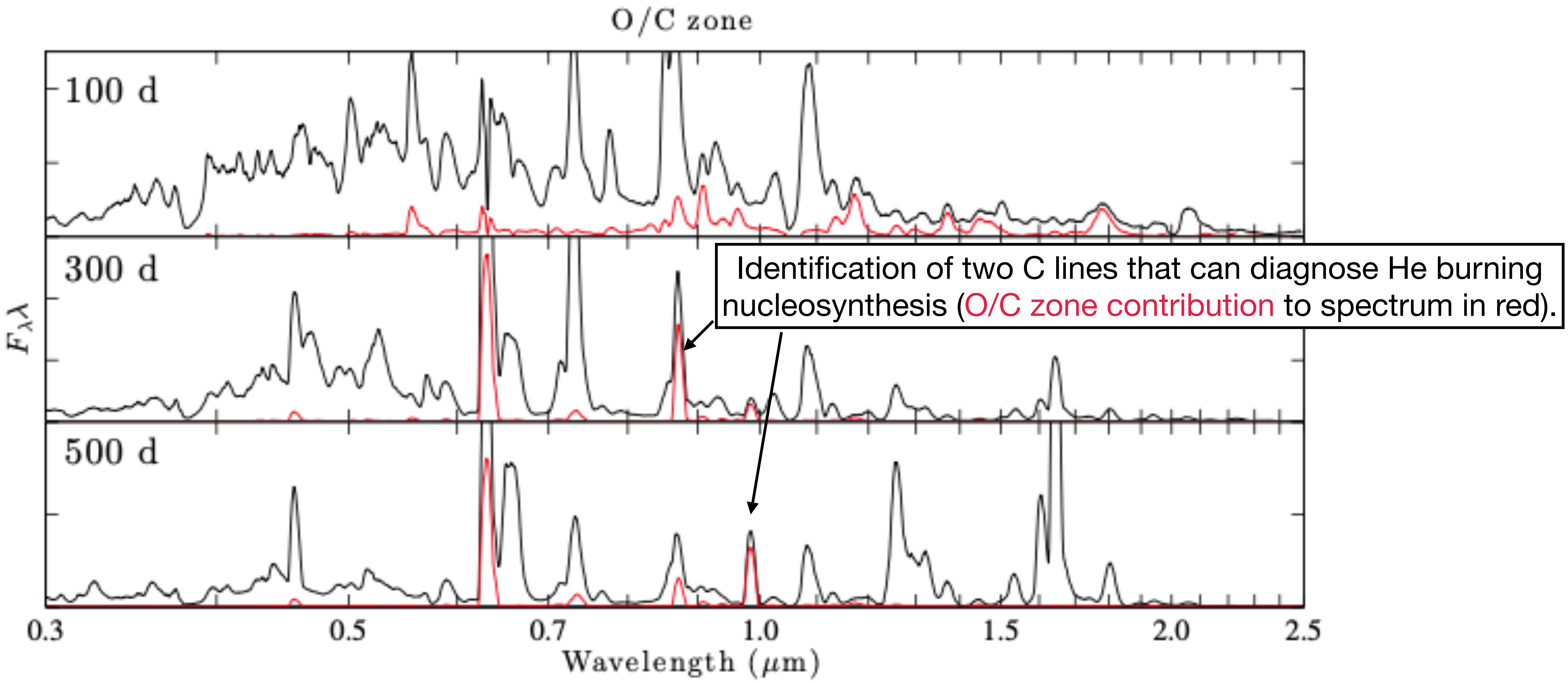

Line expansion opacity can stay important for hundreds of days

This means UV and blue optical region needs to be modelled with radiative transfer.

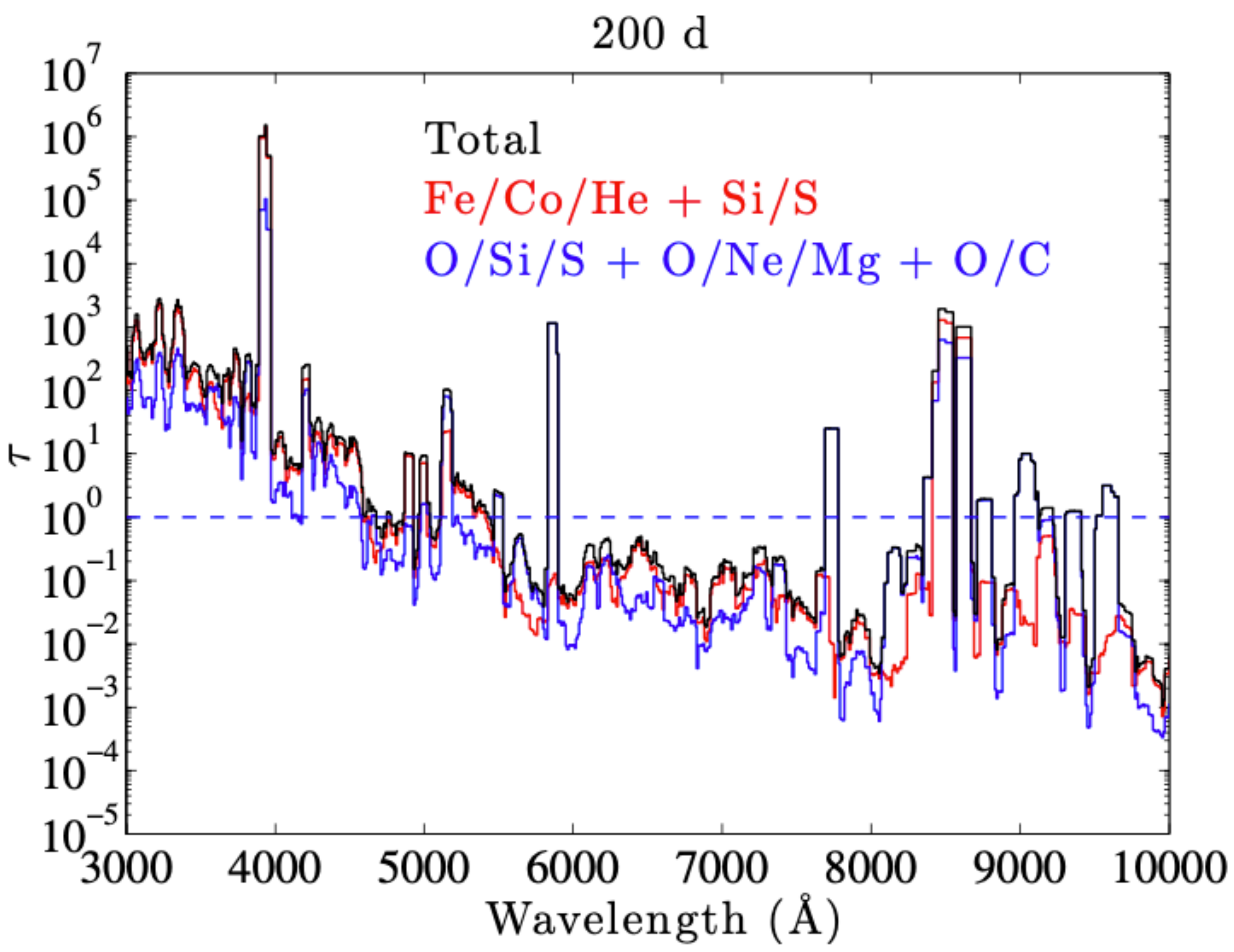

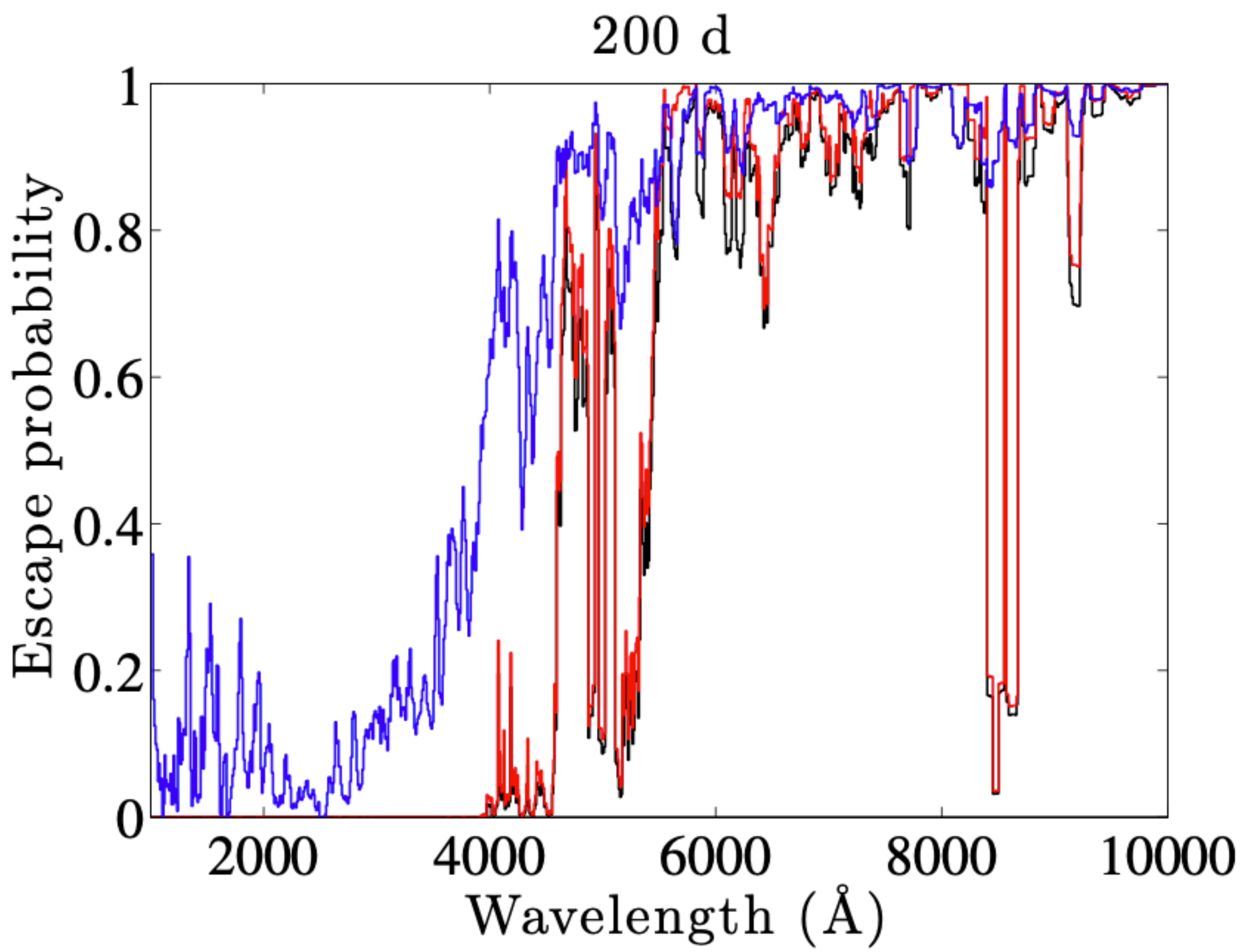

Uniform composition: $\tau_\lambda = \kappa_\lambda^{line,exp} \rho R$

Jerkstrand 2015

Modelling SESN nebular spectra

Mysterious "Hα" emission recently understood to be [N II] 6548, 6583 emission from the He/N zone.

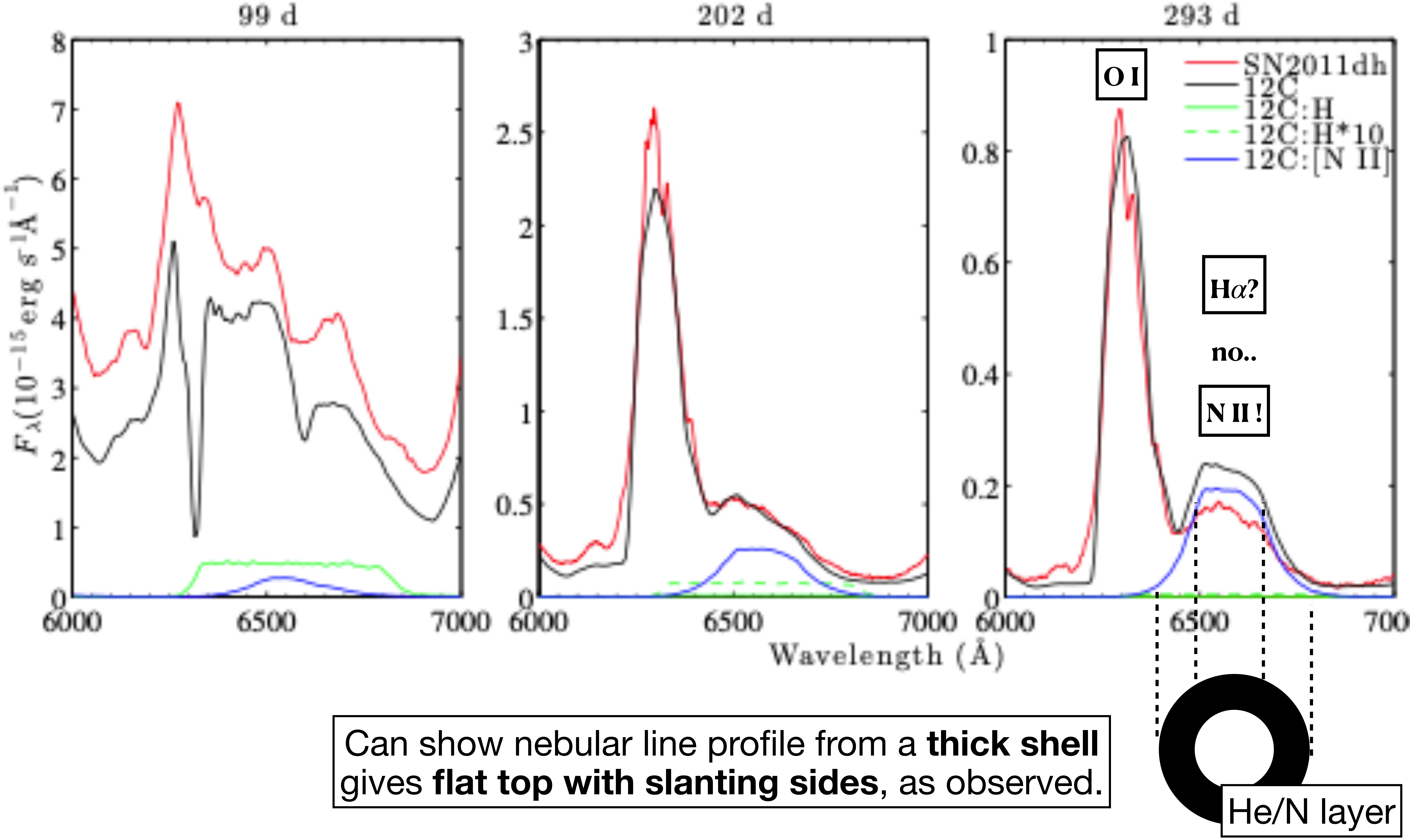

Can show nebular line profile from a **thick shell** gives **flat top with slanting sides**, as observed.

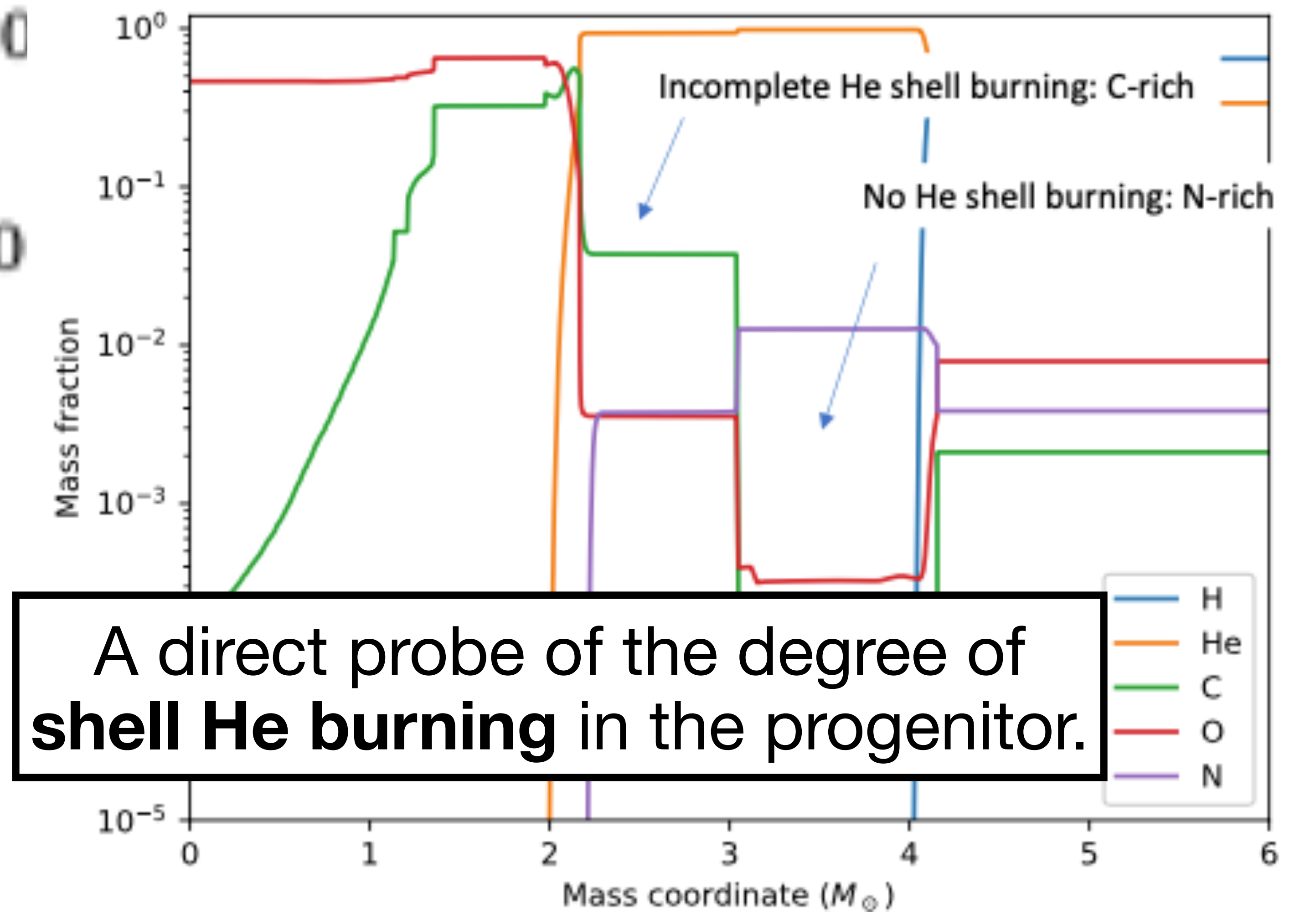

A direct probe of the degree of **shell He burning** in the progenitor.

Jerkstrand 2015

Modelling SESN nebular spectra

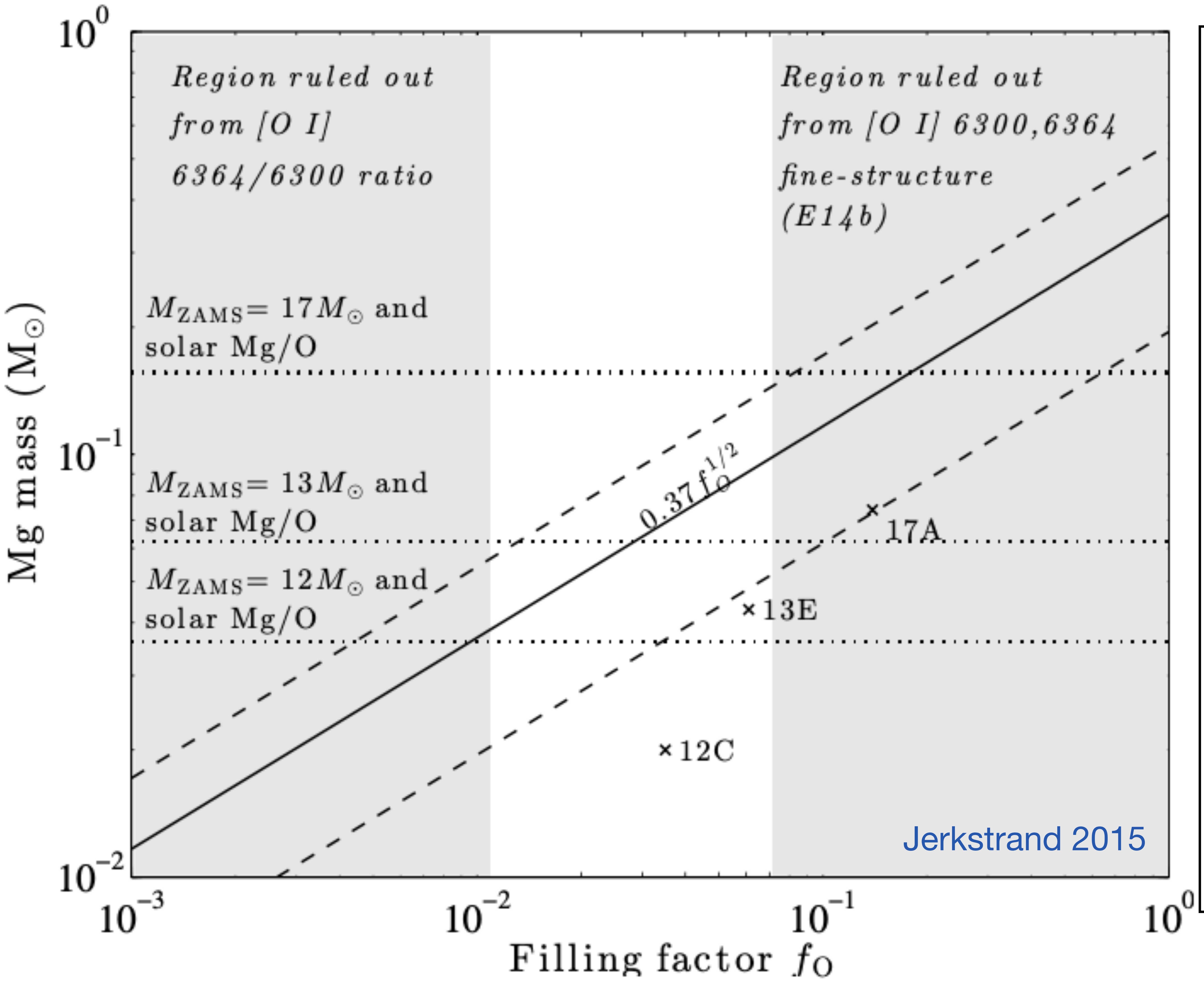

Can we test stellar evolution nucleosynthesis?

One example:

Models show Mg almost always mainly in Mg II form.

Then, a Mg I recombination line luminosity follows

$$L = Vn_{Mg}n_e\alpha_{eff}h\nu = M_{Mg}n_e\alpha_{eff}h\nu$$

where α_{eff} is the effective (total) recombination rate (cm^3 s^{-1}) to the upper level.

Using Mg I 1.50 μm, a pure recombination line, has demonstrated that massive stars indeed make the Mg needed to explain its solar abundance.

Only $n_e f_O^{-1/2}$ determinable from other constraints —> $M(Mg)$ vs f_O relation